2F

PNL-4489
UC-70

Methyl Iodide Sorption by Reduced Silver Mordenite

R. D. Scheele
L. L. Burger
C. L. Matsuzaki

June 1983

Prepared for the U.S. Department of Energy
under Contract DE-AC06-76RLO 1830

Pacific Northwest Laboratory
Operated for the U.S. Department of Energy
by Battelle Memorial Institute

Battelle

PNL-4489

DISCLAIMER

PACIFIC NORTHWEST LABORATORY
operated by
BATTELLE
for the
UNITED STATES DEPARTMENT OF ENERGY
under Contract DE-AC06-76RLO 1830

Printed in the United States of America
Available from
National Technical Information Service
United States Department of Commerce
5285 Port Royal Road
Springfield, Virginia 22161

NTIS Price Codes
Microfiche A01

Printed Copy

Pages	Price Codes
001-025	A02
026-050	A03
051-075	A04
076-100	A05
101-125	A06
126-150	A07
151-175	A08
176-200	A09
201-225	A010
226-250	A011
251-275	A012
276-300	A013

PNL-4489
UC-70

METHYL IODIDE SORPTION BY REDUCED SILVER MORDENITE

R. D. Scheele
L. L. Burger
C. L. Matsuzaki

June 1983

Prepared for the U.S. Department of Energy
under Contract DE-AC06-76RLO 1830

Pacific Northwest Laboratory
Richland, Washington 99352

CONTENTS

FIGURES

TABLES

ACKNOWLEDGMENTS

We would like to thank G. F. Piepel and M. W. Bowen for their help in designing the experimental plan and performing the statistical analysis of the data, F. T. Hara and A. W. Lautensleger for their analytical help, L. D. Maki for typing the report, and S. E. King for her editorial advice.

SUMMARY

At the Pacific Northwest Laboratory (PNL), we performed two sets of experiments to determine the effects of pertinent operational parameters and gas compositions on organic radioiodine [in particular methyl iodide (CH_3I)] capture by silver mordenite (AgZ). In the first set of experiments, we studied the effects of 1) hydrogen pretreatment of AgZ, 2) change in particle size of AgZ, and 3) the presence of water in the gas phase. In the second set of experiments we evaluated on a semi-quantitative basis the effects of nitric oxide (NO), nitrogen dioxide (NO_2), superficial face velocity, and temperature on CH_3I capture by reduced (hydrogen pretreated) silver mordenite (Ag°Z).

These studies have shown that AgZ, especially Ag°Z, is an effective trap for CH_3I. However, its effectiveness varies with changes in operational parameters and is affected by other gases found in the process off gas of a nuclear reprocessing plant. Optimum trapping efficiency was achieved with Ag°Z rather than AgZ, 20-40 mesh Ag°Z rather than 0.16 cm extrudate, moisture in the gas stream, higher temperatures up to 200°C, absence of NO, and lower superficial face velocities down to 3.75 m/min. Additionally, CH_3I can be converted to elemental iodine (I_2) in the presence of NO or NO_2 by controlling the operational parameters. Since I_2 is easier to trap than organic iodides, this should improve trapping efficiency.

INTRODUCTION

Radioiodine arises from the generation of electricity by nuclear power. Because iodine-131 has such a short half-life (8 days), its release must be controlled for only 200 days. Iodine-129, however, with a half-life of 1.6×10^7 years, is still present in significant amounts at 200 days. The primary control point for radioiodine in the nuclear fuel cycle is at a nuclear fuel reprocessing plant (FRP). The principal release form is elemental iodine (I_2); however, organic iodides are produced by reactions with organic contaminants in the dissolver off-gas and vessel vent systems. The predominant compound formed by these reactions is methyl iodide (CH_3I), which may amount in some systems to several percent of the total iodine in the process off gas (POG).

Various technologies have been developed for the capture of radioiodine. Included in these are caustic scrubbing, mercuric nitrate-nitric acid scrubbing, hyper-azeotropic nitric acid (20-22 M) scrubbing, and sorption by silver-containing solids. With each the organic iodides are trapped with varying degrees of success. One of the more promising technologies is capture by hydrogen-reduced silver mordenite ($Ag^{\circ}Z$), which has been demonstrated by Thomas et al. (1977) to trap I_2 more efficiently than ionic silver mordenite (AgZ).

This report describes the results of an evaluation of the effects of selected dissolver off-gas constituents, temperature, and face velocity on the capture of CH_3I by $Ag^{\circ}Z$.

PAST WORK

Few workers have evaluated Ag°Z as a trapping agent for volatilized iodine species. Ag°Z was initially suggested and evaluated at the Idaho National Engineering Laboratory (INEL) for elemental iodine capture. Thomas et al. (1977) found that Ag°Z was superior to AgZ in its capacity for I_2 removal. This was confirmed by our studies (Wiemers 1978; Wiemers and Scheele 1979; Scheele, Matsuzaki, and Burger 1981; Scheele 1981). Following this work, Oak Ridge National Laboratory (ORNL) also began a program to evaluate Ag°Z as a trap for organic iodides (Jubin 1980, 1982).

In INEL's final document on their silver mordenite studies, Murphy, Staples, and Thomas (1977) described their results on elemental iodine removal by Ag°Z:

- Elemental iodine loading of Ag°Z is about twice that of AgZ; loadings of 171 ± 17 mg I/g Ag°Z are possible from simulated dissolver off-gas streams (DOG).
- NO has a positive effect on iodine loading.
- NO_2 has a negative effect on iodine loading.
- Water vapor up to 2.4×10^{-3} mole H_2O/L has little or no effect on iodine loading.
- Temperatures between 100 and 250°C have little or no effect on iodine loading.

INEL workers used a 5 cm dia x 15 cm deep bed of 10-20 mesh Ag°Z, a face velocity of 15 m/min, a bed temperature of 150°C, an iodine concentration of 1.2×10^{-5} mole/L, and a termination retention factor (RF) of 10^3 to 10^4. The Ag°Z was prepared by batch treatment at 500°C for 24 hours. They prepared AgZ by ion exchange of sodium mordenite (NaZ).

In the early work performed by PNL, we studied the effects of carrier gas composition, temperature, and zeolite pretreatment on CH_3I capture by AgZ with these results:

- CH_3I capture was equivalent with either nitrogen or air as the carrier gas.
- Increasing the temperature from 100 to 200°C improved CH_3I capture.
- Ag°Z was more efficient than AgZ in capturing CH_3I.
- The presence of water (5×10^{-4} vs 4.3×10^{-6} mole H_2O/L) in the gas phase improved CH_3I capture.
- Dimethyl ether was detected as one of the reaction products in the column effluent.

Work at ORNL on CH_3I capture by Ag°Z has been described by Jubin (1980, 1982). He used 5 cm dia x 10 to 15 cm deep beds of 0.16 cm dia extrudate, a 10 m/min face velocity, bed temperatures ranging from 83 to 275°C, a typical CH_3I concentration of 7×10^{-6} mole CH_3I/L, and a termination RF of 10^3. He prepared his own AgZ by ion exchange of NaZ and also obtained commercially prepared AgZ from Ionex Corporation. He typically generated the Ag°Z by treatment with 4.5% H_2-Ar at 200°C for 24 hours.

A summary of Jubin's conclusions regarding CH_3I capture by Ag°Z is given below:

- Ag°Z is a more efficient trap for CH_3I than AgZ; loadings up to 127 mg I/g Ag°Z are possible.
- CH_3I concentration and the presence of NO and/or NO_2 have no effect.
- Moist air up to 2×10^{-3} mole H_2O/L improves iodine capture.
- Higher temperatures up to 225°C improve loading.
- Higher temperatures increase the length of the mass transfer zone; at 150°C it was 5 to 7.5 cm; at 200°C it was >10 cm.
- Higher temperatures (200 to 500°C) and longer exposure times (24 or 48 hours) for reduction by 100% H_2 increase the size of the metallic silver nodules formed and reduce loading capacity.

- When using Ag°Z produced at higher temperatures, higher loadings were reached with glass filter housings than with stainless steel housings.
- Partially exchanged Ag°Z improved silver utilization.

FACTORS INFLUENCING IODINE SORPTION

The sorption of elemental iodine or organic iodides by Ag°Z from the POG is a complex process whose chemistry is poorly understood. Furthermore, this sorption process can be affected by several operational factors, physical characteristics of Ag°Z, and several constituents of the POG. Several of these are discussed below.

ZEOLITE STRUCTURE

One of the more important factors is the zeolite itself. For this study only silver mordenite made from the synthetic sodium mordenite Zeolon® was used; NaZ is a high silica zeolite of nominal composition $Na_2O \cdot Al_2O_3 \cdot 10\ SiO_2 \cdot 6H_2O$ (Breck 1974). Figure 1 presents a stereo view of its structure. There are two sets of channels. The main ones, which are 6.7 x 7.0Å, i.e. 7Å in pore size, are linked in the same plane by small pockets having apertures of 3.6 Å (Breck 1974). The effective pore sizes could be changed slightly by substituting Ag for Na. The pore size limits access to the interior of the AgZ. In order for iodine to be sorbed it must pass through the pore openings, and its ability to enter the pores is limited by its molecular size or kinetic diameter. For example, I_2 has a kinetic diameter of 5Å (see Table 1), and we estimate that CH_3I has a kinetic diameter of ~6Å [extrapolating Kennard's (1938) value for CH_3Br]. For these iodine species, mordenite may be one-dimensional; i.e., the molecule may not be able to enter the small channels.

Although blockage of the main channels is common in natural mordenites as a result of impurities or crystal faults, it does not appear to be a problem with the synthetic material Zeolon®. Of the eight Na atoms of the unit cell, four are in small cavities and four randomly situated in the large channels. All are apparently replaceable with Ag ions; however, they are obviously not equally accessible. We discuss other considerations for using AgZ and Ag°Z in a document on the recycling of AgZ by hydrogen reduction (Burger and Scheele 1982).

® Trademark of the Norton Company.

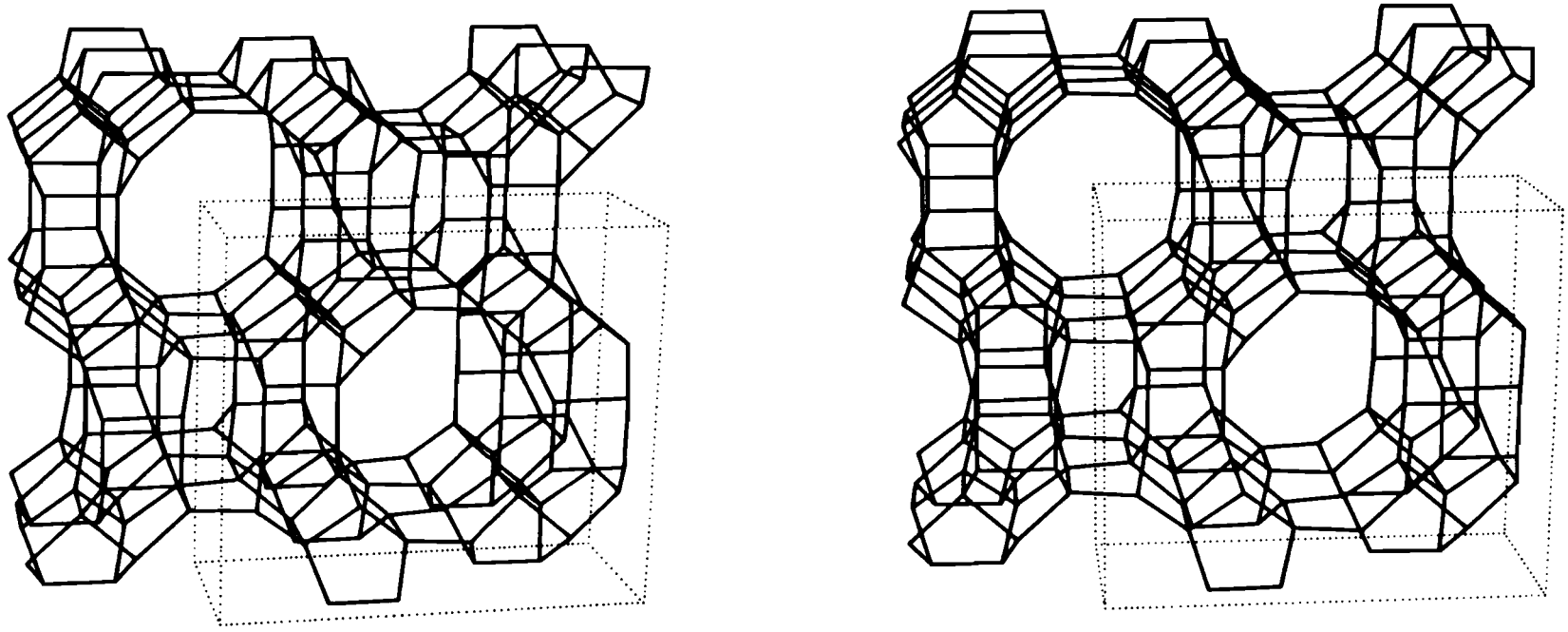

FIGURE 1. Stereo View of NaZ (Reprinted with Permission from Meier and Olson 1971, Copyright 1971 American Chemical Society)

TABLE 1. Critical Diameters for Some Molecules of Interest

Molecule	Critical Diameter, Å				
	Breck[a]	Hirschfelder[b]	Glasstone[c] (Diffusion)	Glasstone[c] (Viscosity)	Kennard[d]
Ar	3.40	3.42			
H_2O	2.65				4.60
CO_2	3.3	3.9	4.38	4.60	4.59
O_2	3.46	3.5	3.64	3.61	3.61
N_2	3.64	3.7	3.84	3.75	3.75
NO	3.17	3.5			
N_2O	3.3	3.8			
Cl_2	3.2	4.1			
Br_2	3.5	4.3			
I_2		5.0	4.6		
HCl			2.86		4.46
HBr			3.16		
HI		4.1	3.50		
CH_4		3.8	3.2		4.14
CH_3OH		3.6			
CH_3Cl		3.4			
CH_3Br					5.85
H_2	2.89		2.72	2.74	2.74

(a) Breck (1974).
(b) Hirschfelder, Curtiss, and Bird (1954).
(c) Glasstone and Bell (1946).
(d) Kennard (1938).

MOLECULAR SIEVE EFFECTS

One of the major industrial uses of zeolites is as a molecular sieve. Different gaseous molecules introduced into a column of zeolite will behave differently within the bed due to their size. Some will pass easily through the pore opening and others will not. The latter molecules will leave the bed first. Table 1 presents some critical diameters for several molecules, some

present in our system. Of the major constituents, the largest molecules of interest are I_2 and CH_3I; there may also be small concentrations of higher organic iodides. The other molecules in our system such as the components of air (N_2, O_2, Ar, CO_2, and H_2O) are all smaller than the large aperture, and several are smaller than the small aperture. Ignoring electrostatic effects or chemical reactions, their size allows them to enter and leave at will. This is also true for NO and probably NO_2, both of which are present in the POG. I_2 and CH_3I will be only slightly hindered in entering and leaving the large pores. It appears that sieving effects of the zeolite will be by the small pores.

Thus all of the molecules in the POG will be free to enter the large pores and potentially be adsorbed or react with the silver within the large pores. Access to the silver in the small pores will be limited to the smaller molecules such as O_2 and NO. Adsorption or the presence of different compounds within the pores could reduce the ability of Ag°Z or AgZ to sorb iodine species by limiting their access into the pore and to the reactive silver sites. The adsorption of water, however, could enhance iodine sorption by mobilizing silver ions in a micro-solution within the zeolite's pores; this effect should be most influential in the ionic form, AgZ. Water may, of course, take part in the chemical reactions.

HYDROGEN PRETREATMENT OF AgZ

It should be mentioned that particles of silver are scattered throughout the Ag°Z. (See Figure 2, which is a scanning electron micrograph of iodine-loaded Ag°Z.) During reduction, the silver migrates from the pores and agglomerates, forming particles up to 2 μm dia (Coleman and Scheele 1981; Daniel, Coleman, and Scheele 1980). Thus, much of the silver is not contained within the zeolite pores. The extent of silver migration and the size of these agglomerates will depend on a number of factors, including water content at the time of reduction, and the temperature and time for reduction (Minachev and Isakov 1976). Our studies indicate that the I_2 is preferentially absorbed in these Ag particles rather than in the zeolite matrix. Therefore, the silver

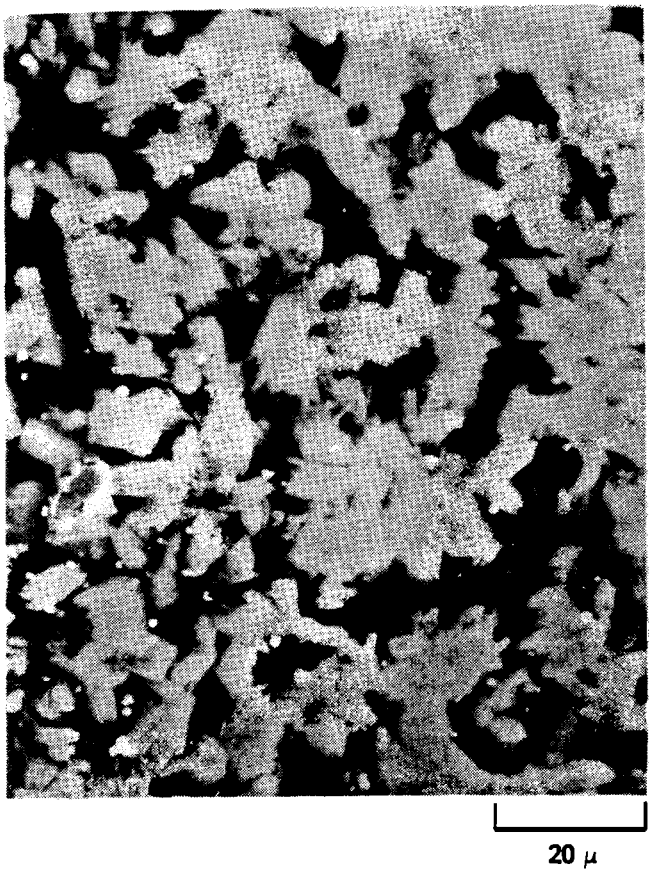

FIGURE 2. Scanning Electron Micrograph of Iodine-Loaded Ag°Z

should be more accessible to the I_2 in Ag°Z than in AgZ, provided that the Ag particles are not too big.

Jubin's (1982) work indicates that the hydrogen reduction conditions and exposure time used for preparing Ag°Z affect the ability of Ag°Z to capture CH_3I. The longer the hydrogen pretreatment and the higher the temperature, the poorer the CH_3I sorption. Jubin attributes this to the larger particle size of Ag metal formed at the more extreme conditions. In other work (Burger and Scheele 1982), we found erratic trapping behavior for I_2 during repeated loading and hydrogen reduction cycles.

CHEMICAL FACTORS

In addition to the factors just discussed, a large number of competing chemical reactions can occur among the reactive components in the zeolite and in the POG which could affect I_2 retention by AgZ or Ag°Z.

Iodine Sorption (Previous Studies)

Donner and Tamberg (1971, 1972) studied the reaction between CH_3I and silver zeolite type X (AgX) and found that methanol and dimethyl ether were formed. The following reactions were proposed:

$$CH_3I + H_2O + Ag^+ \rightarrow AgI + CH_3OH + H^+$$

$$CH_3I + CH_3OH + Ag^+ \rightarrow AgI + CH_3OCH_3 + H^+$$

In their earlier paper they also report that when C_2H_5I is sorbed by AgX, diethyl ether forms, suggesting a similar sorption mechanism with ethanol as an intermediate.

We performed some preliminary work on the chemistry of I_2 and CH_3I sorption by silver containing sorbents. Differential scanning calorimetry (DSC), thermogravimetric analysis (TGA), scanning electron microscopy (SEM) coupled with x-ray fluorescence elemental analysis, and ESCA-Auger spectroscopy were used to characterize iodine sorption reactions and their products and/or to determine the stability of I_2 on the silver sorbents. The results of these studies were discussed in Burger and Scheele (1981) and Scheele and Burger (1981).

NO_x Behavior on Zeolites

Since NO and NO_2 are reactive species, their behavior when adsorbed by zeolites could significantly affect how well iodine is sorbed. Breck (1974) referenced several works on NO or NO_2 adsorption by zeolites. These are discussed in the following.

Addison and Barrer (1955) reported that NO disproportionates upon adsorption in Ca- and Na-rich forms of chabazite, faujasite, mordenite, and a synthetic zeolite with mordenite-like molecular sieve properties. Chao and

Lumsford (1971a, 1971b) found also that NO, upon adsorption by zeolite Y, disproportionates. They reported the following disproportionation reaction:

$$4\ NO \rightleftarrows N_2O + N_2O_3$$

Studying CaY, NaY, HY, and decationized Y zeolites at room temperature, Chao and Lumsford identified the adsorbed species N_2O, NO_2^+, N_2O_3, NO_3^-, a nitrito complex, and nitrite. The final products were N_2O and NO_2. At low temperatures N_2O_2, NO, and disproportionation products were found.

Kasai and Bishop (1972) used electron spin resonance (ESR) spectroscopy to study NO adsorption on NaY, BaY, and ZnY and found that the initial spectra were broad and poorly defined, but after the samples had stood for several days, the spectra became sharp and well defined. They concluded that N_2O_3 was initially formed by disproportionation, but it ionized due to the internal field of the zeolite.

Pietzak and Wood (1970) found NO_2 adsorbed in calcium zeolite type X (CaX) exhibited hindered motion. Adsorbed NO_2 molecules (about 11 per cavity) are essentially dimerized. The single NO_2 molecule surrounded by several N_2O_4 molecules is shielded from interacting with surface cations.

Thermodynamic Considerations

Several potential reactions and their free energies are presented in Table 2. The first set of reactions (1 through 16) are potential iodine absorption reactions. The next set (17 through 22) are reactions between oxides of nitrogen and metallic silver which would compete with iodine sorption; note that NO in reaction 17 could reduce Ag_2O, which may be present in partially reduced Ag°Z. However, the subsequent reactions in the table suggest oxidation to Ag_2O or Ag^+ as predominant. The third set (23 through 30) are reactions between AgI, the optimum silver-iodine species for retention, and the oxides of nitrogen. Included are reactions with such species as N_2O_3 and N_2O_4, which may be adsorption products of NO and NO_2.

Many reactions in set I are thermodynamically favorable for I_2 or CH_3I capture by Ag°Z or AgZ. The iodine species produced are AgI or $AgIO_3$. In

TABLE 2. Reaction Free Energies for Some Possible Reactions in Ag°Z

	Reaction	ΔG_{RX} [a] kJ/mole Ag 300°K	400°K	500°K
	Set I.			
1	$Ag + 1/2\ I_{2(g)} \rightleftarrows AgI$	-76.0	-70.4	-66.4
2	$Ag_2O + I_{2(g)} \rightleftarrows 2\ AgI + 1/2\ O_2$	-22.3	-13.8	-5.45
3	$AgNO_3 + 1/2\ I_{2(g)} \rightleftarrows AgI + 1/2\ O_2 + NO_{2(g)}$	4.47	-14.1	-32.7
4	$2\ Ag + 2\ CH_3I_{(g)} \rightleftarrows 2\ AgI + C_2H_{6(g)}$	-105[b]	-98[c]	-91[c]
5	$Ag + CH_3I_{(g)} + H_2O_{(g)} \rightleftarrows AgI + CH_3OH_{(g)} + 1/2\ H_2$	-21.8[b]	-15[c]	-7.9[c]
6	$Ag + CH_3I_{(g)} + CH_3OH_{(g)} \rightleftarrows AgI + CH_3OCH_{3(g)} + 1/2\ H_2$	-40.8[b]	-32[c]	-23[c]
7	$Ag^+_{(aq)} + CH_3I_{(g)} + H_2O_{(g)} \rightleftarrows AgI + CH_3OH_{(g)} + H^+_{(aq)}$	-99.0[b]	-82[c]	-66 [c]
8	$Ag^+_{(aq)} + CH_3I_{(g)} + CH_3OH_{(g)} \rightleftarrows AgI + CH_3OH_{(g)} + H^+_{(aq)}$	-118[b]	-99[c]	-81[c]
9	$2\ Ag + I_{2(g)} + 3/2\ O_2 \rightleftarrows AgI + AgIO_3$	-93.22[b]	-74[c]	-55[c]
10	$2\ Ag + I_{2(g)} + 3\ NO \rightleftarrows AgI + AgIO_3 + 3/2\ N_2$	-223.25[b]	-202[c]	-181[c]
11	$2\ Ag + I_{2(g)} + 3/2\ NO_{2(g)} \rightleftarrows AgI + AgIO_3 + 3/4\ N_2$	-132.10[b]	-117[c]	-103[c]
12	$Ag_2O + I_{2(g)} + O_2 \rightleftarrows AgI + AgIO_3$	-87.81[b]	-72[c]	-56[c]
13	$Ag_2O + I_{2(g)} + 2\ NO \rightleftarrows AgI + AgIO_3 + N_2$	-174.5[b]	-157[c]	-140[c]
14	$Ag_2O + I_{2(g)} + NO_{2(g)} \rightleftarrows AgI + AgIO_3 + 1/2\ N_2$	-113.73[b]	-101[c]	-88[c]

TABLE 2. (contd)

	Reaction	ΔG_{RX} [a] kJ/mole Ag 300°K	400°K	500°K
15	$7\ NO + 2\ CH_3I_{(g)} \rightleftarrows I_{2(g)} + 2\ CO_2 + 3\ H_2O_{(g)} + 7/2\ N_2$	-1075[b]	-1079[c]	-1084[c]
16	$7\ NO_{2(g)} + 4\ CH_3I_{(g)} \rightleftarrows I_{2(g)} + 4\ CO_2 + 6\ H_2O_{(g)} + 7/2\ N_2$	-841[b]	-853[c]	-865[c]
	Set II.			
17	$2\ Ag + NO_{2(g)} \rightleftarrows Ag_2O + NO$	12.3	11.8	11.2
18	$2\ Ag + 1/2\ O_2 \rightleftarrows Ag_2O$	-5.36	-2.07	1.13
19	$Ag + NO_{2(g)} + 1/2\ O_2 \rightleftarrows AgNO_3$	-80.4	-56.3	-33.7
20	$2\ Ag + NO \rightleftarrows Ag_2O + 1/2\ N_2$	-48.7	-44.8	-41.0
21	$Ag + N_2O_{4(g)} \rightleftarrows AgNO_3 + NO$	-40.7	-41.5	-43.9
22	$Ag + N_2O_{3(g)} \rightleftarrows AgNO_3 + 1/2\ N_2$	-169	-158	-148
	Set III.			
23	$AgI + NO \rightleftarrows Ag + 1/2\ I_{2(g)} + 1/2\ N_2 + 1/2\ O_2$	-10.7	-15.0	-17.7
24	$2\ AgI + NO \rightleftarrows Ag_2O + I_{2(g)} + 1/2\ N_2$	27.2	25.5	25.5
25	$2\ AgI + NO_{2(g)} \rightleftarrows Ag_2O + I_{2(g)} + NO$	88.1	82.2	77.6
26	$AgI + 2\ NO_{2(g)} \rightleftarrows AgNO_3 + 1/2\ I_{2(g)} + 1/2\ N_2 + 1/2\ O_2$	-55.6	-43.5	-31.1
27	$AgI + 2NO_{2(g)} \rightleftarrows AgNO_3 + 1/2\ I_{2(g)} + NO$	30.8	41.9	52.9
28	$AgI + N_2O_{4(g)} \rightleftarrows AgNO_3 + 1/2\ I_{2(g)} + 1/2\ N_2 + 1/2\ O_2$	-51.5	-56.5	-61.5
29	$AgI + N_2O_{4(g)} \rightleftarrows AgNO_3 + 1/2\ I_{2(g)} + NO$	35.2	28.9	22.5

TABLE 2. (contd)

Reaction	ΔG_{RX} (a) kJ/mole Ag		
	300°K	400°K	500°K
30 $AgI + N_2O_{3(g)} \rightleftharpoons AgNO_3 + 1/2\ I_{2(g)} + 1/2\ N_2$	-92.9	-87.2	-81.6

(a) Calculated based on data from Barin and Knacke (1973) or Barin, Knacke, and Kubaschewski (1977), except as noted.
(b) Calculated based on data for 298°K from Latimer (1956).
(c) Calculated using equation $\Delta G = \Delta H + AT$.

other work (Burger and Scheele 1981), sorbed I_2 was released at temperatures lower than the decomposition or volatilization temperatures of either compound, suggesting the presence of a silver-iodine complex.

The first set of reactions show that NO and NO_2 enhance the I_2 capture process, but in the second section the general impact of NO or NO_2 is detrimental. It is obvious that the presence of NO_x greatly complicates zeolite chemistry. In the second section we find that NO_2 endothermically oxidizes Ag to Ag_2O, which has a less energetically favored reaction with I_2; however, if NO is also present in the gas stream, this oxidation will not occur. Murphy, Staples, and Thomas (1977) attributed the positive effect of NO and the negative effect of NO_2 on I_2 capture to this reaction. However, in another case, NO will exothermically oxidize Ag to Ag_2O (reaction 20). The remaining reactions in the second set of reactions are all exothermic and should all compete with iodine sorption reactions; note that the silver products will also react with I_2.

In the third set of reactions, there are several which favor release of I_2 from AgI. Again, the oxides of nitrogen tend to destabilize iodine retention. Two reactions presented in Table 1 show oxidation of CH_3I by NO and NO_2 to form I_2. Both reactions are strongly exothermic and should improve trapping efficiency, since I_2 is more easily trapped than CH_3I.

Not considered in this analysis is the presence of other halogen species such as Cl_2 or Br_2, which could displace trapped iodine. Strachan (1978) analyzed some old iodine absorbers (silver reactors) from the Hanford Purex Plant and found that they were loaded principally with Cl.

OPERATIONAL PARAMETERS

Other factors affecting iodine sorption are operational parameters of the Ag°Z bed. These include Ag°Z particle size, temperature, and four factors which are closely interrelated: face velocity, bed diameter, bed length, and residence time.

A smaller particle size Ag°Z would be expected to be more efficient because of both increased surface area and a smaller diffusion path. The free volume does not change appreciably, nor does gas flow; i.e., the flow is expected to be laminar for the particle sizes and flows used here. This was verified by measurement of flow-pressure drop.

The effect of temperature will depend on what the controlling reactions are: they may be physical, e.g., diffusion and/or adsorption and have a relatively low activation energy, E_a; or chemical, with much higher E_a values. In any case, we would expect them to be linear with respect to exp (-1/T).

Bed diameter and length are interrelated with face velocity and residence time. In this study, we ignored the potential effects of bed sizing and residence time and arbitrarily selected a bed diameter and a length to exceed the expected mass tranfer zone, thus lumping these factors into one variable, superficial face velocity. Face velocity would be expected to have a linear effect if there is no change in mechanism.

The factors selected for study were presence of NO, presence of NO_2, temperature, and superficial face velocity. The experimental program was selected to determine which factors affected CH_3I sorption.

EXPERIMENTAL CONSIDERATIONS

We performed two sets of experiments, the first using a 2.5 cm dia x 15 cm deep bed, and the second using a 5.0 cm dia x 18.0 cm deep bed. The basic system is diagrammed in Figure 3. The operating conditions for each experiment are presented in Table 3 and Table 4, respectively. The containers for the mordenite and other glass components in the system were borosilicate glass. Other materials used in construction were stainless steel and plastic tubing. The plastic (Teflon® and Tygon®) tubing was restricted to locations upstream from the heaters.

To insure constant temperature throughout the bed, three heat tapes were used, and the bed insulated with a ceramic fiber blanket. Thermocouples were placed in each bed segment. Initially, we used proportional temperature controllers. Later, a small laboratory computer monitored and controlled bed segment temperatures. In addition to temperature monitoring and control, the computer also initiated experiments and monitored and recorded other experimental conditions such as flow rates and dew point.

We pretreated each bed with air for 16 hours at the operating temperature. This insured an equilibrium water content and silver oxidation state.

Gas tanks containing ~4 x 10^{-4} mole CH_3I/L N_2 were prepared and used as the CH_3I source. The influent CH_3I concentration used in our experiments was 1.3 x 10^{-5} moles CH_3I/L. The CH_3I concentration varied with each individual tank so it was necessary to adjust flows based on standard analyses made prior to each run.

NO_2 was prepared by reacting 1 part NO with 9 parts O_2 in a 1 L or 3 L holdup flask. For the experiments with NO experiments, the NO conversion to NO_2 by reaction with air was minimized by introducing the NO just prior to the top of the mordenite bed.

® Teflon is a trademark of E. I. du Pont de Nemours & Co.
® Tygon is a trademark of the Norton Company.

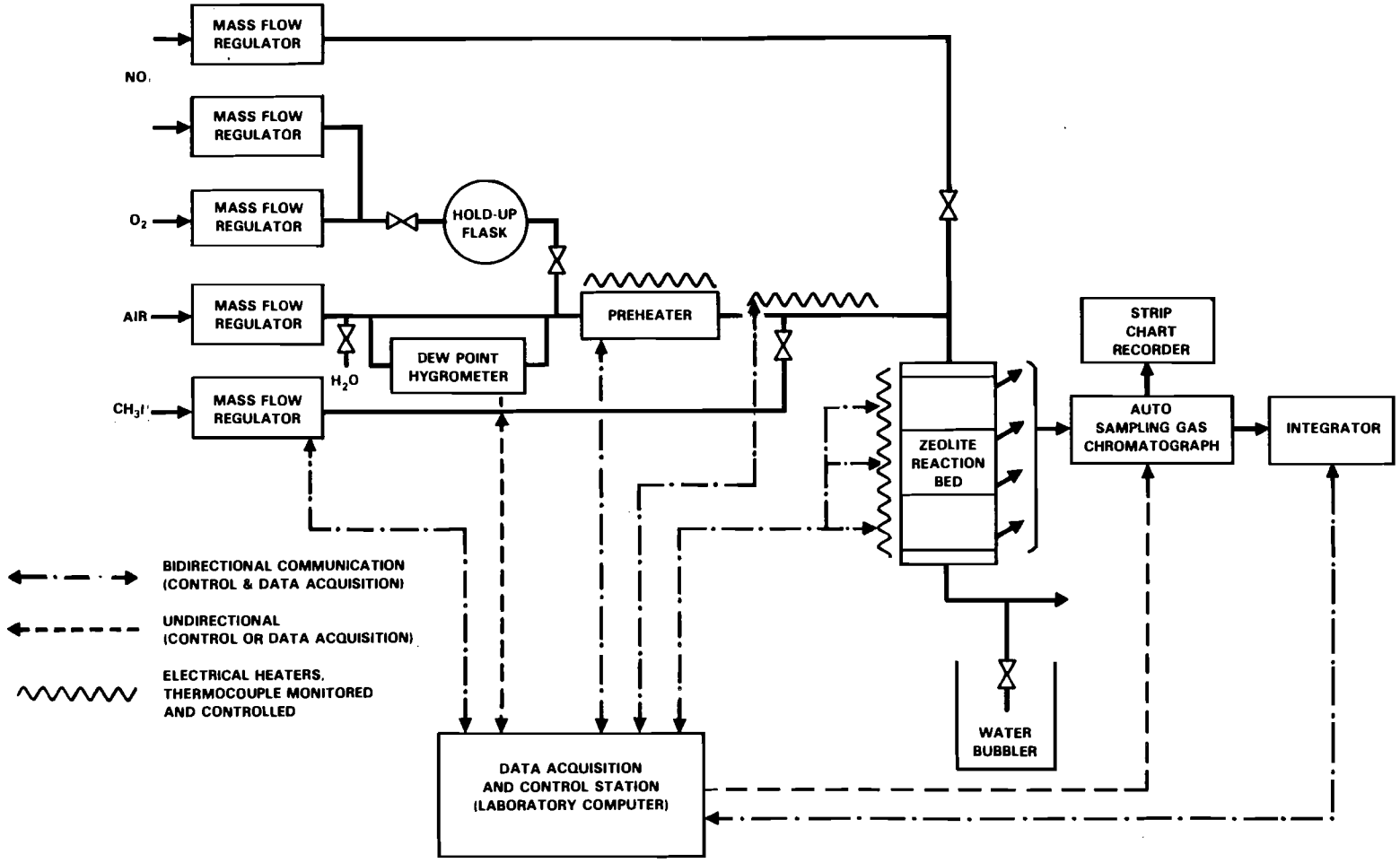

FIGURE 3. Experimental Apparatus for CH_3I Capture by Silver Mordenite (AgZ or Ag°Z)

TABLE 3. Operating Parameters for 2.5 cm Dia Bed

Bed length, cm	15
Bed diameter, cm	2.54
Bed material	AgZ or Ag°Z
Particle size	20-40 mesh or 0.16 cm diameter extrudate
Bed temperature, °C	110, 150, or 200°C
Face velocity, m/min	7.5
Carrier gas	Air
CH_3I concentration, mole/L	1.3×10^{-5}
H_2O concentration, mole/L	
Laboratory air	$\sim 5 \times 10^{-4}$
Tank air	4×10^{-6}
NO concentration, mole/L	0 or 8×10^{-4}
NO_2 concentration, mole/L	0 or 8×10^{-4}

TABLE 4. Operating Parameters for 5.0 cm Dia Bed

Bed length, cm	18
Bed diameter, cm	5.08
Bed material	Ag°Z
Particle size	10-16 mesh
Bed temperature, °C	86, 116, 152, or 200
Face velocity, m/min	3.75, 7.5, or 15
Carrier gas	Air
CH_3I concentration, mole/L	1.3×10^{-5}
H_2O concentration, mole/L	$\sim 5 \times 10^{-4}$
NO concentration, mole/L	0, 5.2×10^{-5} or 4×10^{-4}
NO_2 concentration, mole/L	0, 2.6×10^{-5} or 4×10^{-4}

We used laboratory air with a nominal water content of ~5 x 10^{-4} mole H_2O/L as our air source. In a few early experiments, we used tank air having a water content of 4 x 10^{-6} mole H_2O/L. The laboratory air was pumped using an oil-free pump. In preliminary tests with the 5 cm dia bed, we used an oil lubricated pump. However, oil was observed in the delivery lines. Since this could contaminate the mordenite bed, we switched to completely oil-free components.

The AgZ was procured from Ionex Corporation presized. The AgZ used in the 2.5 cm dia bed was 20-40 mesh and 0.16 cm dia extrudate, while in the 5.0 cm dia bed we used 10-16 mesh (one experiment used 20-40 mesh). The Ag°Z was prepared by heating the AgZ at 300°C in a dry N_2 stream for 3 to 4 hours followed by heating at 500°C in flowing H_2 for 24 hours.

A gas chromatograph with an auto-sampling valve measured the CH_3I concentration in the influent and bed segment effluents (see Figure 3). For the 2.5 cm dia bed, samples were taken of the influent and after each 5.0 cm segment. For the 5.0 cm diameter bed, samples were taken of the influent, after the first 8.0 cm, and then after each of the remaining two 5 cm bed segments. We used a 2 m Pora-Pak QS® 80 x 100 mesh column at 200°C with a He flow of 100 mL/min. This gave a CH_3I retention time of 7.5 minutes. A photoionization detector with a 10.5 eV lamp was used. A normal sampling cycle for the entire bed required 50 minutes. Methyl iodide standards were run prior to and after each experiment.

When NO or NO_2 was present, some or all of the CH_3I was converted to I_2. We monitored I_2 progress through the bed using tissue paper dipped in a starch solution. When I_2 was present, the paper turned the characteristic blue-purple color of the starch-iodine complex. This method allowed us to detect an RF of ~100.

We used the integrated input CH_3I to calculate the average bed loading. For selected experiments, each bed segment was analyzed by F. T. Hara and A. W. Lautensleger of PNL using x-ray fluorescence to determine the iodine loadings.

® Trademark of Waters Associates, Inc.

Species other than NO, NO_2 or CH_3I were detected in the off gas. While determination of other chemical species was beyond the scope of this project, possibilities are dimethyl ether or methanol, as mentioned earlier.

TABLE 5. Summary of 2.5 cm dia Bed Studies

Exp. No.	Bed Material	NO, mole/L	NO_2, mole/L	Temp., °C	Face Velocity, m/min	H_2O, mole/L	Average Loading @ RF=100, mg I/g AgZ	Iodine Species at Breakthrough
1-1	0.16 cm extrudate AgZ	0	0	150	15.0 7.5	$\sim 5 \times 10^{-4}$	<5	CH_3I
1-2	20-40 mesh AgZ	0	0	150	3.75	$\sim 5 \times 10^{-4}$	<117	I_2
1-3	20-40 mesh Ag°Z	0	0	150	7.5	$\sim 5 \times 10^{-4}$	139	CH_3I
1-4	20-40 mesh Ag°Z	0	0	150	7.5	4×10^{-6}	30	CH_3I
1-5	20-40 mesh Ag°Z	4×10^{-4}	4×10^{-4}	155	7.5	$\sim 5 \times 10^{-4}$	<135	I_2(a)
1-6	20-40 mesh Ag°Z	4×10^{-4}	4×10^{-4}	155	7.5	$\sim 5 \times 10^{-4}$	191	I_2(a)
1-7	20-40 mesh Ag°Z	8×10^{-4}	0	150	7.5	5×10^{-4}	145	I_2(a)
1-8	20-40 mesh Ag°Z	0	8×10^{-4}	200	7.5	$\sim 5 \times 10^{-4}$	<135	I_2(a)
1-9	20-40 mesh Ag°Z	0	8×10^{-4}	110	7.5	$\sim 5 \times 10^{-4}$	>177	I_2(a)

(a) No CH_3I after first 5 cm bed segment.

EXPERIMENTAL RESULTS

Initial plans were to use a 2.54 cm dia x 15 cm deep bed of 20-40 mesh Ag°Z to evaluate the effects of temperature, NO, and NO_2 on CH_3I capture using a statistical experimental design (2^3 factorial). After some preliminary work (experiments 1-1 through 1-6) and the first three runs of the experimental design (1-7 through 1-9), it was determined that a larger bed and larger mesh size would give more significant results for process design. We increased the bed size to 5.0 cm dia x 18 cm deep and the particle size to 10-16 mesh. Based on our work with the 2.5 cm dia bed, we expanded this experimental design to include a fourth variable, superficial bed velocity. Four experiments (2-1 through 2-4) were performed to measure variability before beginning the statistically designed experimental program (experiments 2-6 through 2-28).

2.5 cm DIA BED STUDY

The experimental parameters and results for the small bed are presented in Table 5. Appendix Figures A.1 and A.2 present CH_3I concentration in the influent and effluents for each 5 cm bed segment as a function of average bed loading for experiments 1-3 and 1-4.

For the other experiments, measurement of CH_3I concentrations was impossible because CH_3I was converted to I_2 in the first bed segment. In comparing these and subsequent data, it may be noted that the maximum theoretical loading, assuming AgI, is about 225 mg I/g zeolite.

From these preliminary studies, several observations can be made:

- If NO or NO_2 was present, the CH_3I was converted to I_2 for Ag°Z; this conversion also occurred for AgZ at a face velocity of 3.75 m/min in the absence of NO_x.
- If there was very little water in the gas stream (4×10^{-6} mole/L), the trapping efficiency of Ag°Z was significantly reduced (compare experiments 1-3 and 1-4).

TABLE 5. Summary of 2.5 cm Dia Bed Studies

Exp. No.	Bed Material	NO, mole/L	NO_2, mole/L	Temp., °C	Face Velocity, m/min	H_2O, mole/L	Average Loading @ RF=100, mg I/g AgZ	Iodine Species at Breakthrough
1-1	0.16 cm extrudate AgZ	0	0	150	15.0 7.5	$\sim 5 \times 10^{-4}$	<5	CH_3I
1-2	20-40 mesh AgZ	0	0	150	3.75	$\sim 5 \times 10^{-4}$	<117	I_2
1-3	20-40 mesh Ag°Z	0	0	150	7.5	$\sim 5 \times 10^{-4}$	139	CH_3I
1-4	20-40 mesh Ag°Z	0	0	150	7.5	4×10^{-6}	30	CH_3I
1-5	20-40 mesh Ag°Z	4×10^{-4}	4×10^{-4}	155	7.5	$\sim 5 \times 10^{-4}$	<135	I_2(a)
1-6	20-40 mesh Ag°Z	4×10^{-4}	4×10^{-4}	155	7.5	$\sim 5 \times 10^{-4}$	191	I_2(a)
1-7	20-40 mesh Ag°Z	8×10^{-4}	0	150	7.5	5×10^{-4}	145	I_2(a)
1-8	20-40 mesh Ag°Z	0	8×10^{-4}	200	7.5	$\sim 5 \times 10^{-4}$	<135	I_2(a)
1-9	20-40 mesh Ag°Z	0	8×10^{-4}	110	7.5	$\sim 5 \times 10^{-4}$	>177	I_2(a)

(a) No CH_3I after first 5 cm bed segment.

- Larger mordenite particles, 0.16 cm dia extrudate, had a poorer trapping efficiency than 20-40 mesh material.
- AgZ was less efficient than Ag°Z even at a lower face velocity (compare experiments 1-2 and 1-3).
- The presence of NO and/or NO_2 (NO_x) had mixed effects on the loading efficiency; experiments 1-3 and 1-5 appear to have comparable loadings, while experiment 1-6 had a much greater loading under identical conditions.
- Temperature had mixed effects on loading.

Because all of the experiments in the statistical experimental plan were not completed, the individual effects of temperature, NO, and NO_2 were confounded, and thus it was difficult to extract any conclusions about any one of these individual effects from this set of data.

5.0-cm DIA BED STUDY

The apparent importance of face velocity suggested that we include it as a parameter. With the help of G. F. Piepel of PNL we set up a 2^4 factorial design with 4 replicates of the center of the hypercube. The replicates are needed to provide an estimate of pure (random) error. In an attempt to have linear response variables, we transformed the temperature and the NO and NO_2 concentrations. The temperature variable $X_T = \exp(-1/T)$ is based on the Arrhenius equation, $k = A \exp(-E_a/T)$, where k is the reaction rate, A is the frequency factor, E_a is the activation energy, and T is temperature in degrees Kelvin.

For the NO and NO_2 transformation variables we assumed that they reacted with CH_3I as shown in equations (15) and (16) in Table 2. The NO_x/CH_3I ratios are roughly 4 and 2, respectively. We therefore adopted the transformations

$$X_{NO} = \left(\frac{[NO]}{-4.1 \times 10^{-4}} \right)^{1/4} \quad \text{and}$$

$$X_{NO_2} = \left(\frac{[NO_2]}{4.1 \times 10^{-4}} \right)^{1/2}$$

The constant 4.1×10^{-4} is the maximum concentration employed in moles/L, and is equivalent to about 1 vol%.

The experimental conditions, average iodine loading at breakthrough (RF = 100), and the iodine species found in the effluent are presented in Table 6. The first four runs 2-1 through 2-4 (Figures A.3 through A.6) were made to measure variability. The parametric study included experiments 2-5 through 2-24. The high temperature experiments were 2-25 through 2-28. Figures A.5 through A.26 are plots of CH_3I concentration in the influent, effluent from the first 8 cm bed segment, and the next two 5 cm bed segments as a function of average bed loading. In some figures the 8 cm bed segment was divided into 3 and 5 cm bed segments. (Figures are not presented for Experiments 2-9, 2-13, and 2-25 because their CH_3I was converted to I_2).

In this set of experiments performed using a larger bed and particle size, we did not typically see total conversion of all of the CH_3I to I_2 in the presence of NO_x as we did with the smaller particle size Ag°Z. We did, however, see total conversion in 2-10 and 2-13, both at 150°C and 3.75 m/min face velocity, one with NO_x absent and the other with NO_x present. Total conversion did occur at 200°C in the presence of NO_x, independent of face velocity. Particle size does affect the efficiency of the CH_3I conversion to I_2 on a silver mordenite bed.

Table 7 presents the results of several confirmatory x-ray fluorescence analyses performed by F. T. Hara and A. W. Lautensleger of PNL. In some cases the loading was not terminated at breakthrough, so the final materials contained more iodine than presented in Table 4. To extrapolate bed segment loadings at an RF of 100, the ratio of the final average loading to the time-based average loading at an RF of 100 was found, and the final loading of each bed segment was divided by this ratio. To illustrate the accuracy of the analysis, the time-based final loading is also presented.

TABLE 6. Summary of 5.0 cm Dia Bed Studies

Exp. No.	NO, mole/L	NO_2, mole/L	Temp., °C	Face Velocity, m/min	Average Loading @ RF=100, mg I/g Ag°Z	Iodine Species at Breakthrough
2-1	0	0	116	15.0	25	CH_3I
2-2	0	0	116	15.0	15	CH_3I
2-3	0	0	116	15.0	29	CH_3I (No I_2 detected)
2-4	0	0	116	15.0	22	CH_3I (No I_2 detected)
2-5	5.2×10^{-5}	2.6×10^{-5}	116	7.5	38	CH_3I (I_2 at 3 cm)
2-6	4.1×10^{-4}	0	152	15.0	19	CH_3I (No I_2 detected)
2-7	0	0	86	15.0	<7	CH_3I (No I_2 detected)
2-8	4.1×10^{-4}	4.1×10^{-4}	152	15.0	63	CH_3I (I_2 at 13 cm)
2-9	0	4.1×10^{-4}	152	3.75	127	I_2 (No CH_3I detected)
2-10	0	0	152	3.75	157	CH_3I and I_2
2-11	5.2×10^{-5}	2.6×10^{-5}	116	7.5	97	CH_3I (I_2 at 13 cm)
2-12	0	4.1×10^{-4}	86	3.75	25	CH_3I (I_2 at 3 cm)
2-13	4.1×10^{-4}	4.1×10^{-4}	152	3.75	93	I_2 (No CH_3I detected)
2-14	4.1×10^{-4}	0	86	3.75	32	CH_3I (No I_2 detected)
2-15	4.1×10^{-4}	4.1×10^{-4}	86	3.75	21	CH_3I (No I_2 detected)
2-16	4.1×10^{-4}	0	86	15.0	15	CH_3I (No I_2 detected)
2-17	5.2×10^{-5}	2.6×10^{-5}	116	7.5	105	CH_3I (I_2 at 3 cm)
2-18	0	0	152	15.0	47	CH_3I (No I_2 detected)
2-19	0	4.1×10^{-4}	152	15.0	55	CH_3I (I_2 at 13 cm)
2-20	0	0	86	3.75	71	CH_3I (No I_2 detected)
2-21	0	4.1×10^{-4}	86	15.0	15	CH_3I (No I_2 detected)
2-22	4.1×10^{-4}	4.1×10^{-4}	86	15.0	6	CH_3I (No I_2 detected)
2-23	4.1×10^{-4}	0	152	3.75	91	CH_3I and I_2
2-24	5.2×10^{-5}	2.6×10^{-5}	116	7.5	47	CH_3I (I_2 at 13 cm)
2-25	4.1×10^{-4}	4.1×10^{-4}	200	3.75	76	I_2 (No CH_3I detected)
2-26	0	0	200	3.75	217	I_2 and CH_3I
2-27	0	0	200	15.0	169	I_2 and CH_3I
2-28	4.1×10^{-4}	4.1×10^{-4}	200	15.0	88	I_2 (No CH_3I detected)

TABLE 7. Summary of Iodine Loading by Bed Segment

Exp. No.	Bed Segment[a]	Estimated[b] Iodine Loading at an RF = 100, mg I/g Ag°Z	Measured Iodine[c] Loading at End of Loading, mg I/g Ag°Z	Time Calculated Iodine Loading at Experiment End, mg I/g Ag°Z
2-5	1A	59	139	
	1B	60	141	
	2	33	80	
	3	8	19	
	Ave	38	90	85
2-11	1A	108	137	
	1B	126	160	
	2	114	144	
	3	44	56	
	Ave	97	123	127
2-17	1A	150	173	
	1B	143	164	
	2	90	104	
	3	55	63	
	Ave	105	121	112
2-24	1A	71	142	
	1B	72	145	
	2	36	71	
	3	18	36	
	Ave	47	94	95
2-25	1A		75	
	1B		91	
	2		122	
	3		82	
	Ave	76[d]	94	76

TABLE 7. (contd)

Exp. No.	Bed Segment[a]	Estimated[b] Iodine Loading at an RF = 100, mg I/g Ag°Z	Measured Iodine[c] Loading at End of Loading, mg I/g Ag°Z	Time Calculated Iodine Loading at Experiment End, mg I/g Ag°Z
2-26	1A	221	232	
	1B	219	230	
	2	219	230	
	3	212	223	
	Ave	217	228	250
2-27	1A	189	216	
	1B	174	199	
	2	177	202	
	3	144	164	
	Ave.	169	193	240
2-28	1A		116	
	1B		108	
	2		100	
	3		62	
	Ave	88[d]	94	88

(a) The bed, when removed, was segmented as 1A, top 3 cm; 1B next 5 cm; 2, next 5 cm; and 3, next 5 cm.
(b) Estimated loading was calculated for each segment by multiplying the measured iodine content on that segment by the ratio of the time-calculated total bed average to the measured total bed average.
(c) Determined by X-ray fluorescence analysis.
(d) Experiment stopped at RF = 100. Time-calculated loading at end. Segment loading should be same as X-ray analysis.

Inspection of the loadings by bed segment shows mass transfer zones ranging from 10 cm (experiment 2-5) to less than 5 cm (experiment 2-26).

As mentioned earlier, the maximum theoretical loading, assuming AgI as the product, is 225 mg I/g AgZ. Experiment 2-26, loaded at 200°C in the absence of NO_x, has nearly the maximum theoretical loading.

DATA ANALYSIS

A statistical analysis of the results was performed by W. M. Bowen of PNL. To determine whether a variable affected CH_3I capture, an extensive analysis of variance (ANOVA) was performed using a statistical computer package.

An ANOVA (e.g., Table 8) attempts to analyze the variation found for a dependent variable (response) by attributing portions of the response variation to independent variables (sources). There are two basic sources of response variation: 1) random or pure error variation, caused by factors which are not or cannot be controlled; and 2) variations caused by changes in the levels of the source variables which were controlled in the experiment.

The theory and methodology of ANOVA is too complex to be discussed here, so we will only provide a brief explanation in general terms. For further information, reading Snedecor and Cochran (1980) is suggested.

ANOVA partitions the total variability in the response variable into portions attributable to each independent variable. The Sum of Squares (SS) or Mean Square (MS) for each independent variable is a measure of the portion of the total variability accounted for by the effect of the independent variable on the response variable. To determine whether the effect of this independent variable is statistically significant, its MS is divided by the Mean Square due to experimental error (MSE). When there is no effect, this ratio follows the F distribution. When there is an effect, the ratio will tend to be larger than an F distributed variable. Thus, the ratio is compared with a value obtained from a Table of the F distribution. The independent variable has a statistically significant effect if the ratio exceeds the table value. The significance level reported in the ANOVA table is the probability of being wrong in concluding that the independent variable actually has an effect beyond variations due to experimental error. Thus, a small significant level provides greater confidence in concluding that there actually is an effect.

The analysis was performed in two phases. The first (Phase 1) analyzed the data from experiments 2-5 to 2-24. The second (Phase II) added the results

TABLE 8. Full Model ANOVA for Phase 1 Analysis

Source		Degrees of Freedom	Sum of Squares	Variance Ratio	Significance Level
Main Effects	NO	1	1681.0	1.44	
	NO_2	1	72.3	<1	
	Temperature (T)	1	13225.0	11.35	0.05
	Face velocity (F)	1	9506.3	8.16	0.10
Two-way Interactions	NOxNO_2	1	462.3	<1	
	NOxT	1	361.0	<1	
	NOxF	1	930.3	<1	
	NO_2xT	1	90.3	<1	
	NO_2xF	1	1156.0	<1	
	TxF	1	1980.3	1.70	
Three-way Interactions	NOxNO_2xT	1	156.3	<1	
	NOxNO_2xF	1	144.0	<1	
	NOxTxF	1	90.3	<1	
	NO_2xTxF	1	36.0	<1	
Four-way Interaction	NOxNO_2xTxF	1	196.0	<1	
	Lack-of-fit	1	1155.0	<1	
	Pure Error	3	3495	MSE = 1165	

from the experiments (2-25 through 2-28) performed at 200°C. The results of each phase were similar, as discussed in detail below. Temperature and face velocity had the greatest effects, NO had a lesser effect, and NO_2 had no effect. The highest iodine loadings were obtained at higher temperatures, lower face velocities, and in the absence of NO. Complex interactions were found between the different independent variables; i.e., the effect of one variable is affected by the level of another variable.

Phase 1 Analysis

Initially an ANOVA was performed to test the significance of the 4 main factors, 6 two-way interactions, 4 three-way interactions, and 1 four-way interaction, and to test for lack-of-fit. A statistically significant main effect indicates that the corresponding factor had a linear effect on the response variable, which is average bed loading at an RF of 100. A significant two-way interaction means that the effect of one variable depends on the level of a second variable and vice versa. The same applies to the three-way and four-way interactions. The lack-of-fit test indicates whether any of the factors had other than simple linear effects.

The results of the initial ANOVA, which are presented in Table 8, indicate that lack-of-fit, the three-way and four-way interactions are not significant. Thus, these could be "pooled" with pure experimental error to provide an improved estimate of pure experimental error and a reduced model tested by ANOVA.

The reduced ANOVA results are presented in Table 9. We find that the temperature (T) and superficial face velocity (F) have significant main effects, and that they interact (TxF symbolizes the interaction of temperature and face velocity). These linear effects and interactions are illustrated in Figures 4 and 5. In the figures the mean bed loadings appear in parentheses.

Figure 4 indicates that bed loading increases with increasing temperature, and this increase is greater at low face velocity. However, the relative loadings $[L(T_2)/L(T_1)]$ are not very different, being slightly greater at the high velocity. The nature of the interdependence of F and T, as seen in Figures 4 and 5, is unclear. From the low loadings at the lower temperature, it is apparent that the silver sites are effectively blocked; i.e., the CH_3I residence time is not adequate at either flow rate.

The main effect of NO and the two-way interactions of NOxF and NO_2xF were significant at the 0.25 level. Figures 6 and 7 show the effects of NO and NO_2 at the two levels of face velocities, respectively. The introduction of NO reduced the mean loading; this effect was greater at 3.75 m/min than at 15 m/min. As discussed in the Phase 2 section, it appears that NO blocked,

TABLE 9. Reduced Model ANOVA for Phase 1 Analysis

Source	Degrees of Freedom	Sum of Squares	Variance Ratio	Significance Level
NO	1	1681.0	2.87	0.25
NO_2	1	72.3	<1	
Temperature (T)	1	13225.0	22.57	0.005
Face Velocity (F)	1	9506.3	16.23	0.005
$NOxNO_2$	1	462.3	<1	
NOxT	1	361.0	<1	
NOxF	1	930.3	1.59	0.25
NO_2xT	1	420.2	<1	
NO_2xF	1	1156.0	1.97	0.25
TxF	1	1980.3	3.38	0.10
Error	9	5272.6	MSE = 585.8	

competed with, or inhibited the reaction of CH_3I with the active sites in Ag°Z. The effect of NO_2 was mixed. At 3.75 m/min, a decrease in mean loading occurred, while at 15 m/min, a slight increase in mean loading occurred. The effect was greater at the low face velocity.

Phase 2 Analysis

In phase 2 all 28 data points were included in the analysis. The same process of eliminating statistically nonsignificant effects and estimating a "pooled" variance was performed. The results of the reduced model ANOVA are presented in Table 10. Because of the incomplete design at 200°C, where we only evaluated the presence or absence of NO_x, the effects of NO and NO_2 are completely confounded at this temperature. Thus the NOxT and NO_2xT two-way interactions are partially confounded for all temperatures. Therefore, for this analysis it was assumed that NO_2xT is negligible based on the Phase I analysis.

Table 10 shows that NO_2 main effect, $NOxNO_2$ and NO_2xT two-way interactions, and the three-way and four-way interactions were nonsignificant. Note

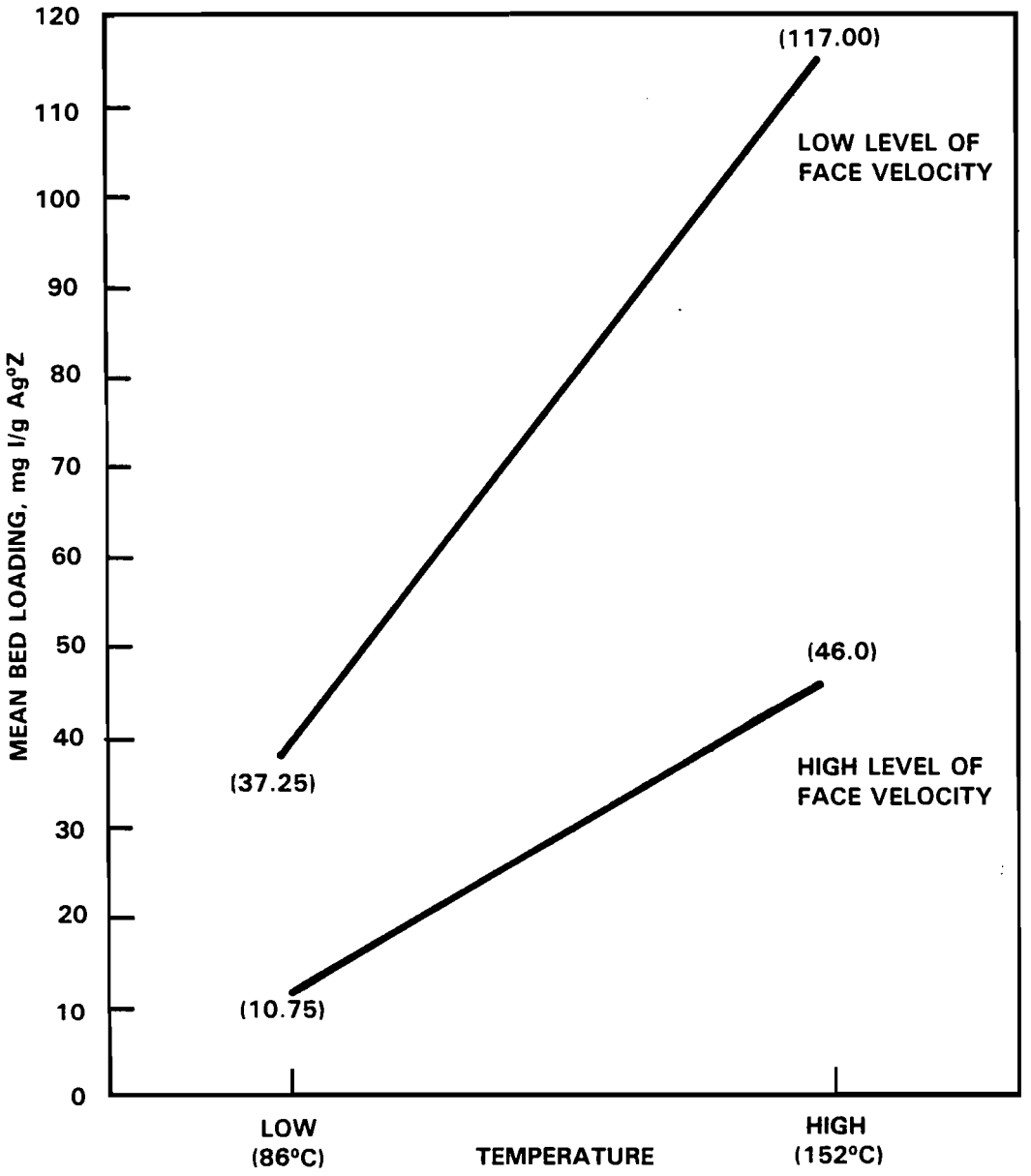

FIGURE 4. Phase 1 Analysis: The Effect of Temperature on CH_3I Capture by Ag°Z at Face Velocities of 3.75 and 15 m/min

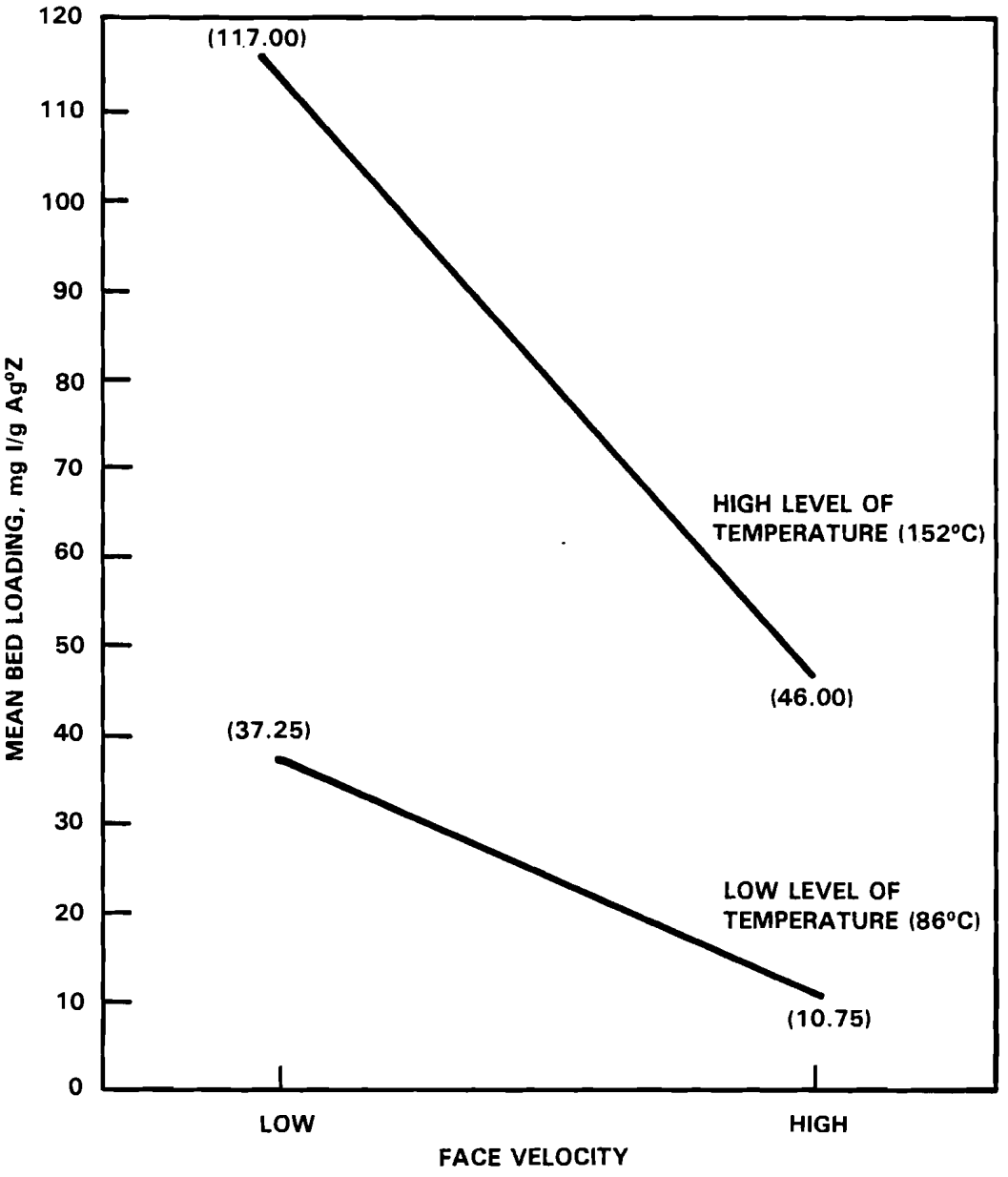

FIGURE 5. Phase 1 Analysis: The Effect of Face Velocity on CH_3I Capture by Ag°Z at 86 and 152°C

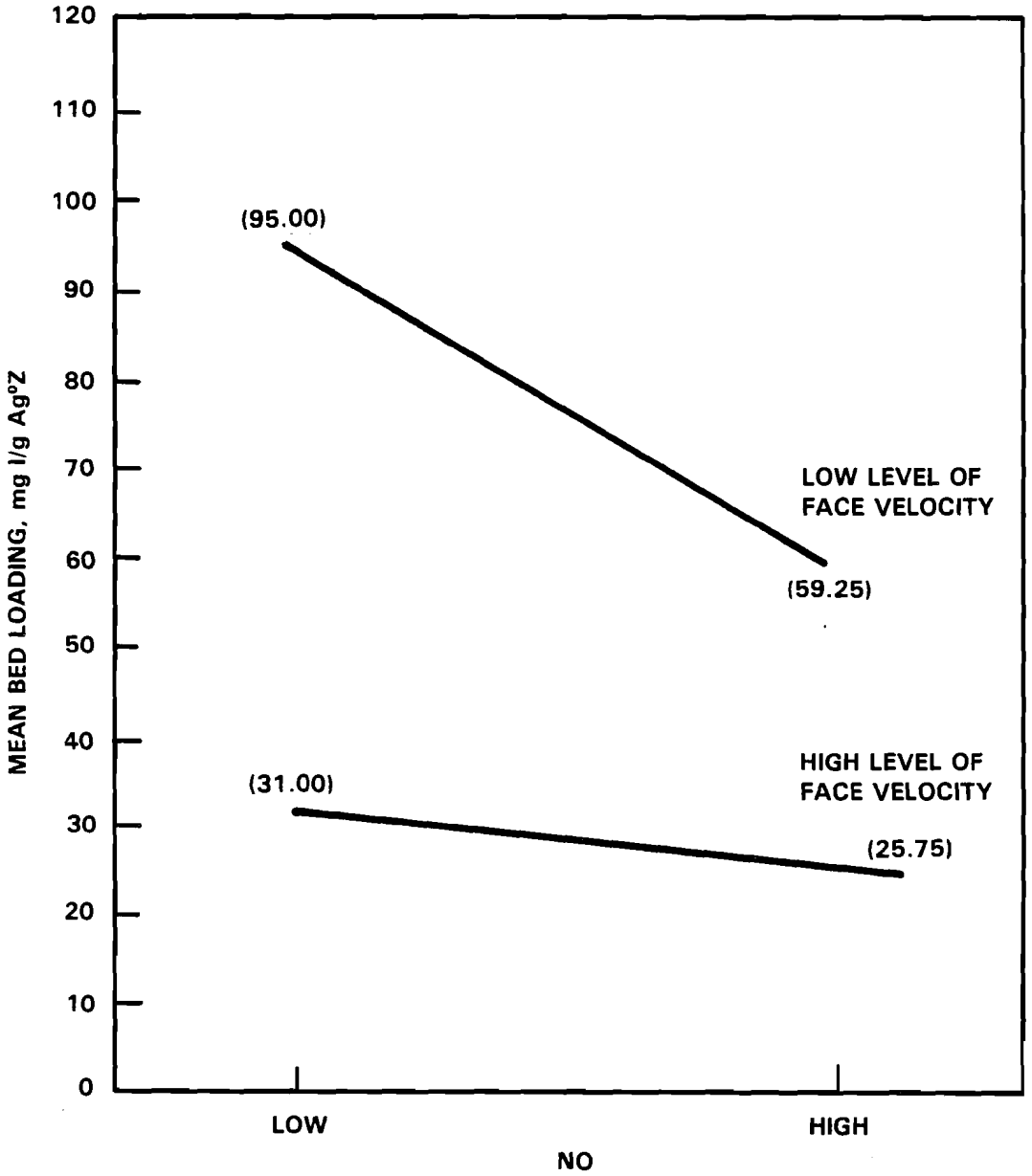

FIGURE 6. Phase 1 Analysis: The Effect of NO on CH_3I Capture by Ag°Z at Face Velocities of 3.75 and 15.0 m/min

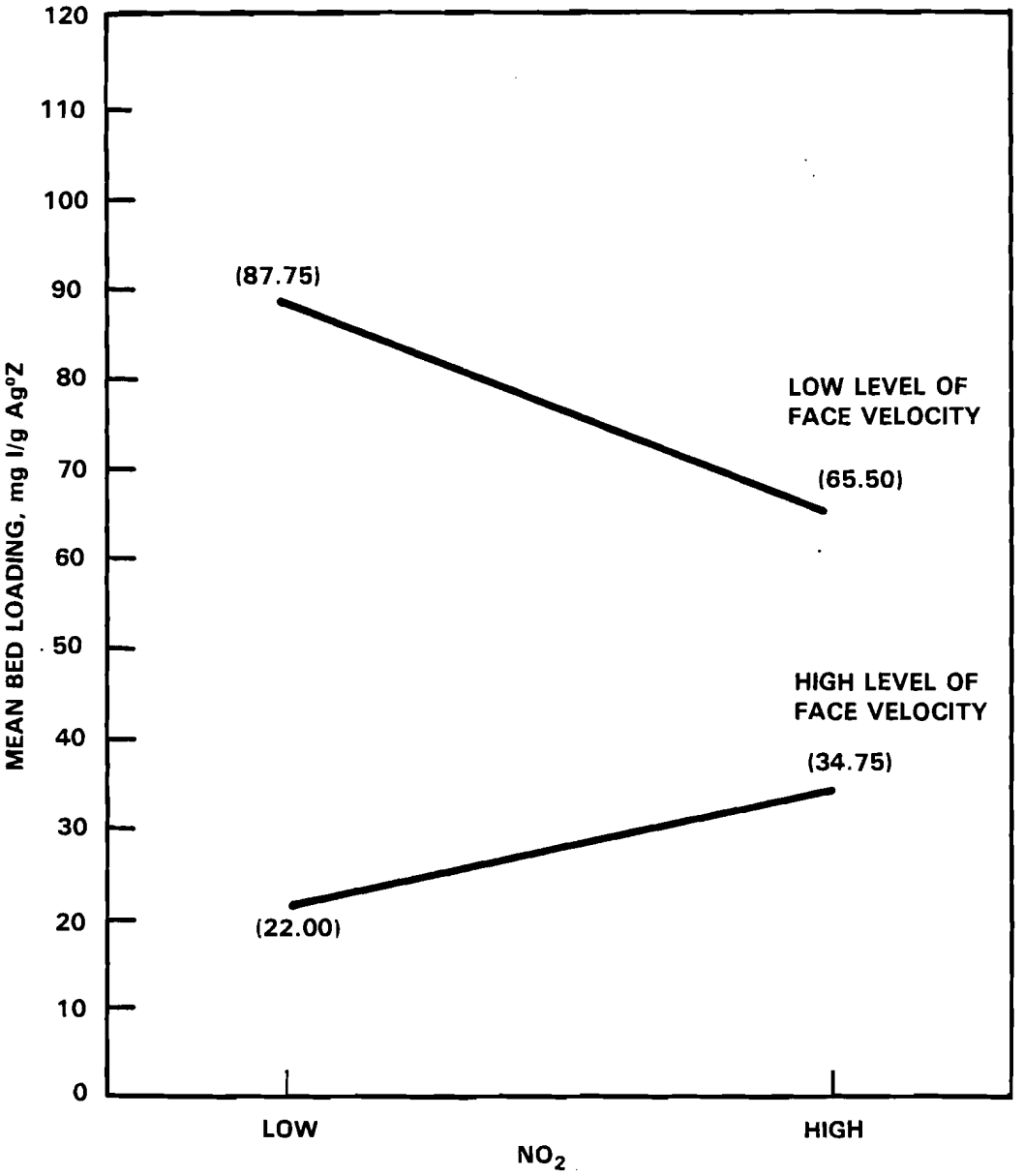

FIGURE 7. Phase 1 Analysis: The Effects of NO_2 on CH_3I Capture by Ag°Z at Face Velocities of 3.75 and 15.0 m/min

TABLE 10. Reduced Model ANOVA For Phase 2 Analysis

Source	Degrees Freedom	Sum of Squares	Mean Sum of Squares	Variance Ratio	Significance Level
NO	1	8133	8133	20.49	0.0005
Temperature (T)	2	34365	17183	43.28	0.0005
Contrast 1 (C1)	(1)	13225	13225	33.31	0.0005
Contrast 2 (C2)	(1)	21140	21140	53.25	0.0005
Face velocity (F)	1	12225	12225	30.87	0.0005
NOxT	2	5871	2936	7.40	0.01
NOxC1	(1)	361	361	1	
NOxC2	(1)	5510	5510	13.88	0.005
NOxF	1	2690	2690	6.78	0.025
NO_2xF	1	3118	3118	7.85	0.025
TxF	2	2400	1200	3.02	0.10
C1xF	(1)	1980	1980	4.99	0.05
C2xF	(1)	420	420	1.06	
Lack-of-fit	1	4562	4562	11.49	0.005
Error	16	6351	MSE = 397		

also in Table 10 that temperature is partitioned into two contrasts. Contrast 1 is the same analysis used in Phase 1. Contrast 2 (C2) compares the average of the means at 86 and 152°C with the mean at 200°C.

There are three significant terms in Table 10 which are not in Table 9: lack-of-fit, C2, and NOxC2. Figure 8 illustrates the NOxT interaction. When NO was present, bed loading sharply increased as T was increased from 152 to 200°C. At 1% NO, there is only a slight increase between 152 and 200°C.

Figures 9 and 10 illustrate the NOxF and NO_2xF two-way interactions, respectively. These are consistent with the results from Phase 1 (see Figures 6 and 7). At high face velocity, 15 m/min, NO and NO_2 have no effect, while at low face velocity, they significantly reduce the mean loading.

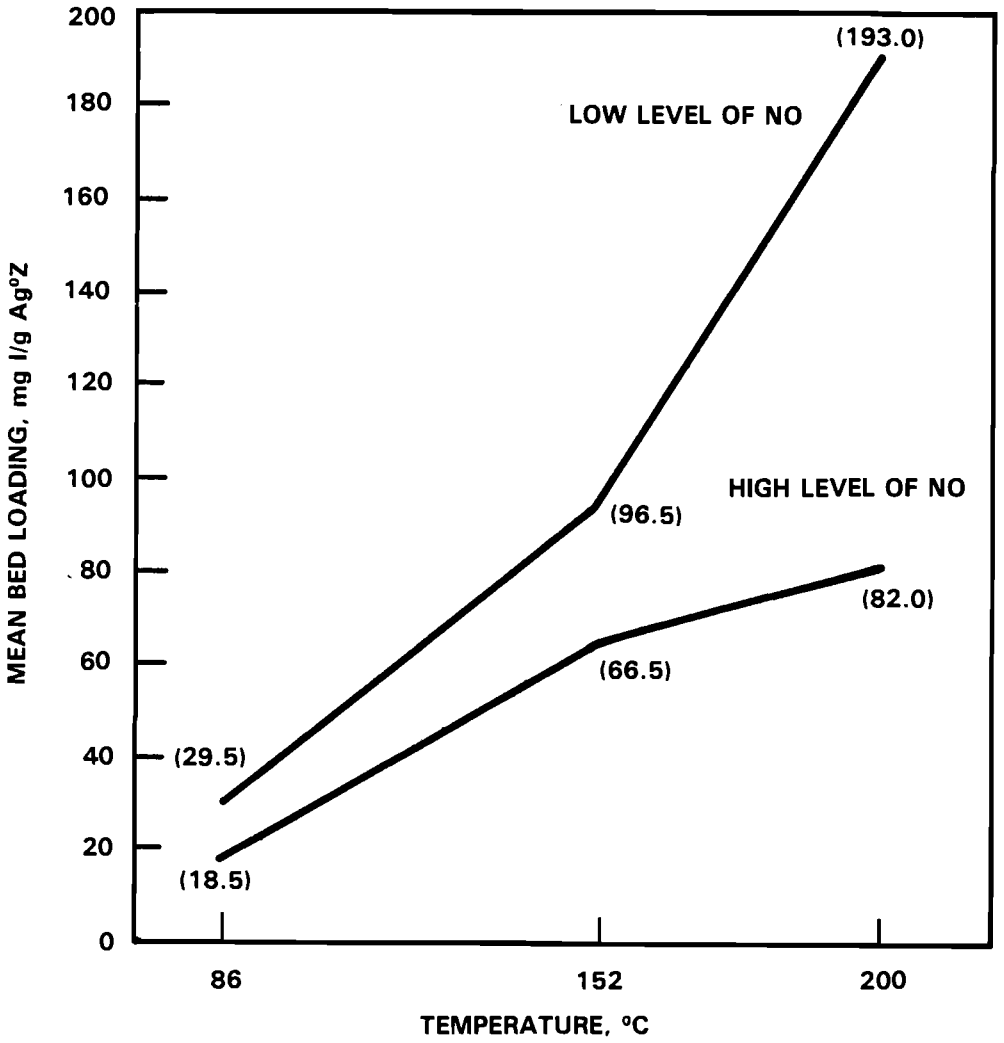

FIGURE 8. Phase 2 Analysis: The Effect of Temperature on CH_3I Capture by Ag°Z at 0 and 2 vol% NO

The typically negative effects seen for the oxides of nitrogen, especially NO, can be attributed to a number of factors. Included in this list are reaction or complex formation between the NO_x species, their condensation products, or their disproportionation products with the active silver; or reaction with the iodine-silver forms; or physical blockage of the zeolite pores, hindering access of the iodine to the active silver sites. Too little information is available to define the correct mechanism or combination of mechanisms.

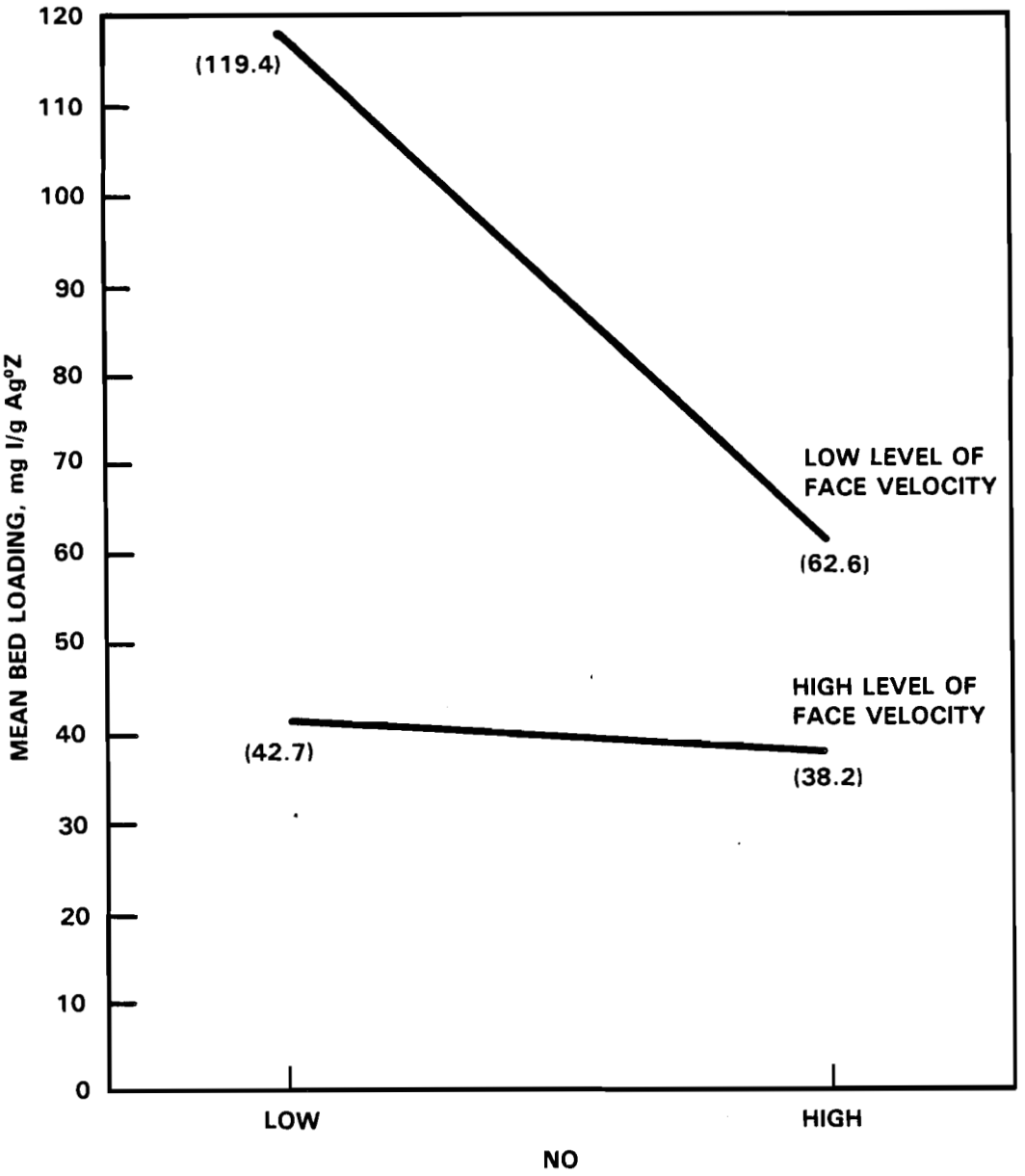

FIGURE 9. Phase 2 Analysis: The Effect of NO on CH_3I Capture by Ag°Z at Face Velocities of 3.75 and 15.0 m/min

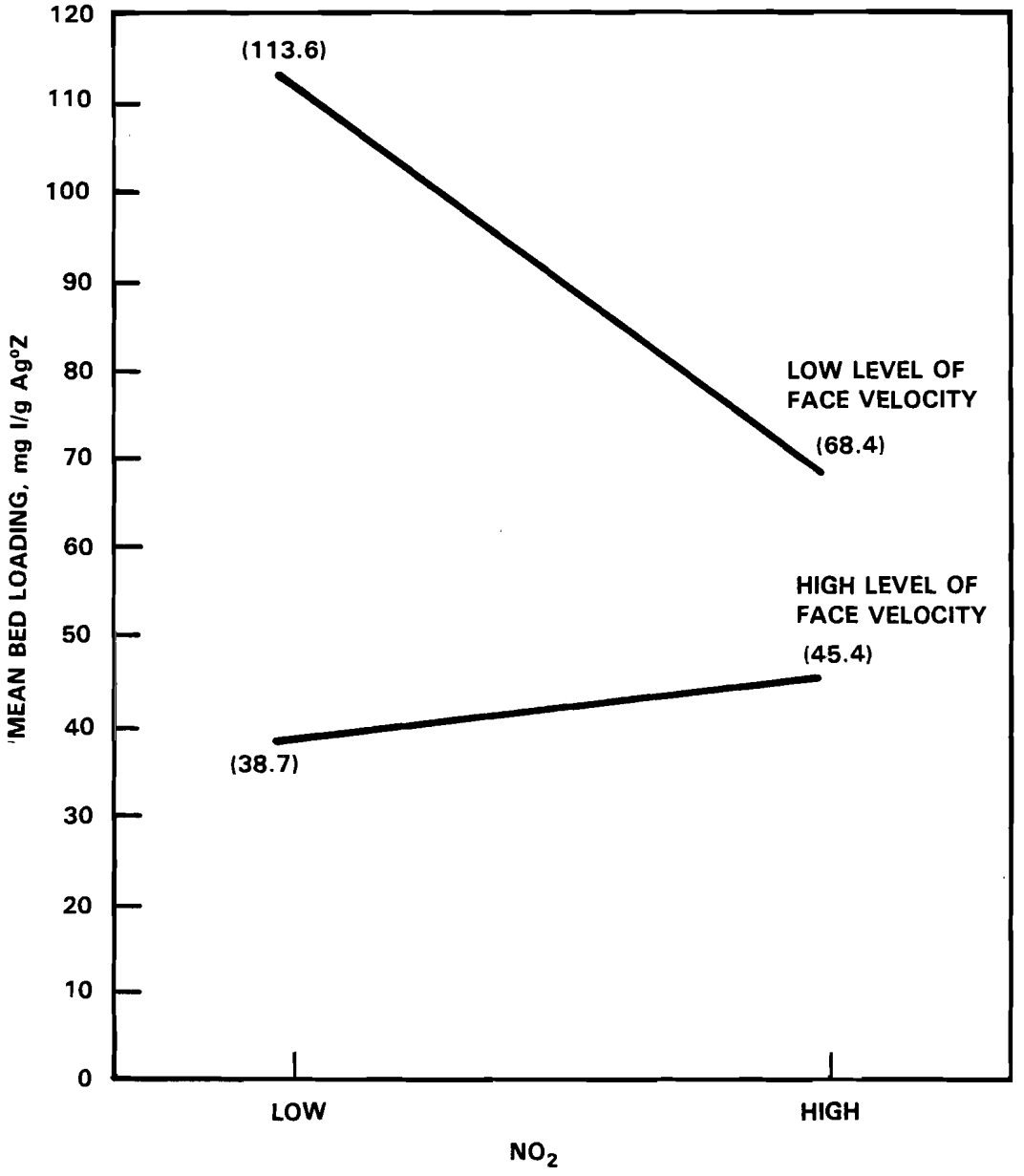

FIGURE 10. Phase 2 Analysis: The Effect of NO_2 on CH_3I Capture by Ag°Z at Face Velocities of 3.75 and 15.0 m/min

Figures 11 and 12 are two illustrations of the TxF interaction. When T was set at 86 or 200°C, face velocity had only a slight effect; however, when T was at 152°C, a sharp decrease in loading was seen when F was increased.

The loading at breakthrough increases with temperature over the complete range, as expected. If we assume that rates are proportional to loadings, admittedly questionable, then the calculated activation energies are small, (5 to 10 kcal). The fact that the loadings are not linear with the transformed temperature, i.e., exp (-1/T), over the complete range is not surprising in view of the interactions just discussed.

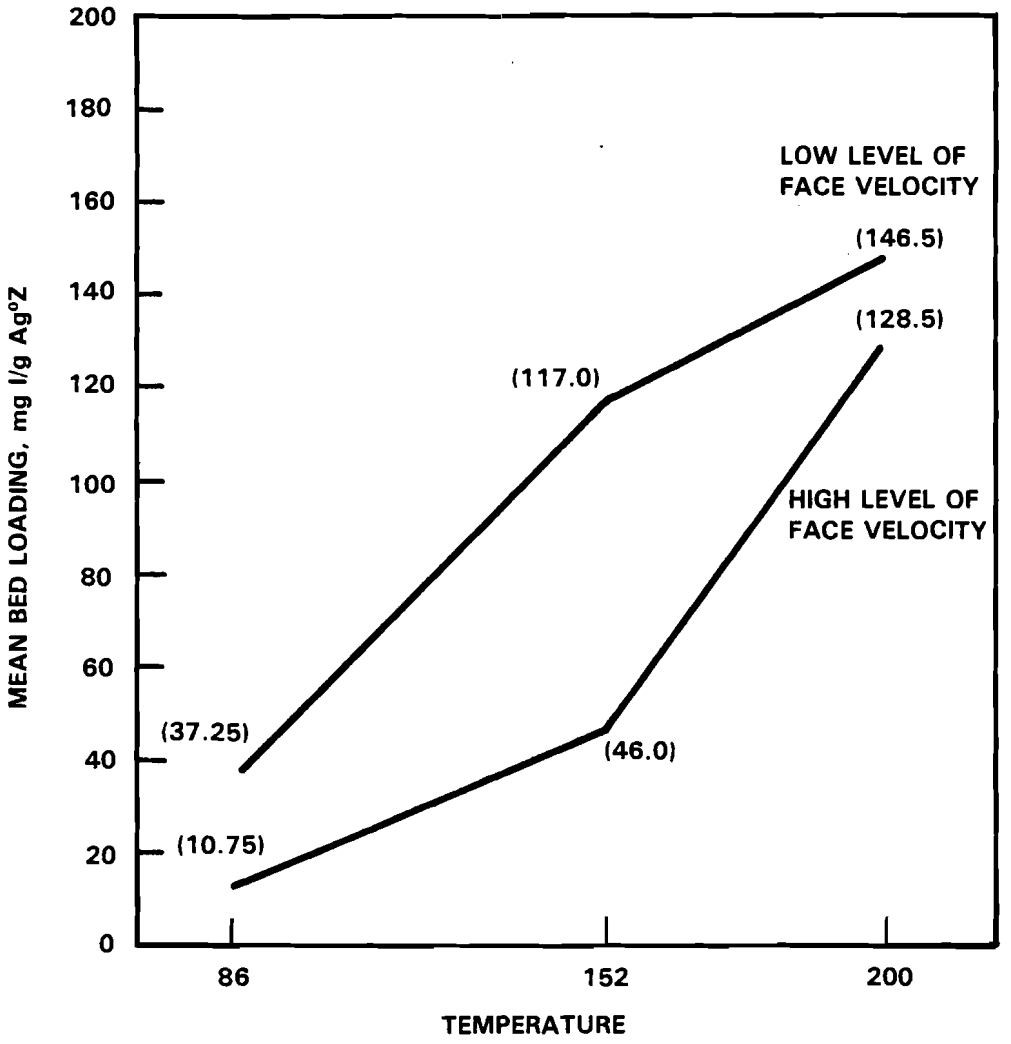

FIGURE 11. Phase 2 Analysis: The Effect of Temperature on CH_3I Capture by Ag°Z at Face Velocities of 3.75 and 15.0 m/min

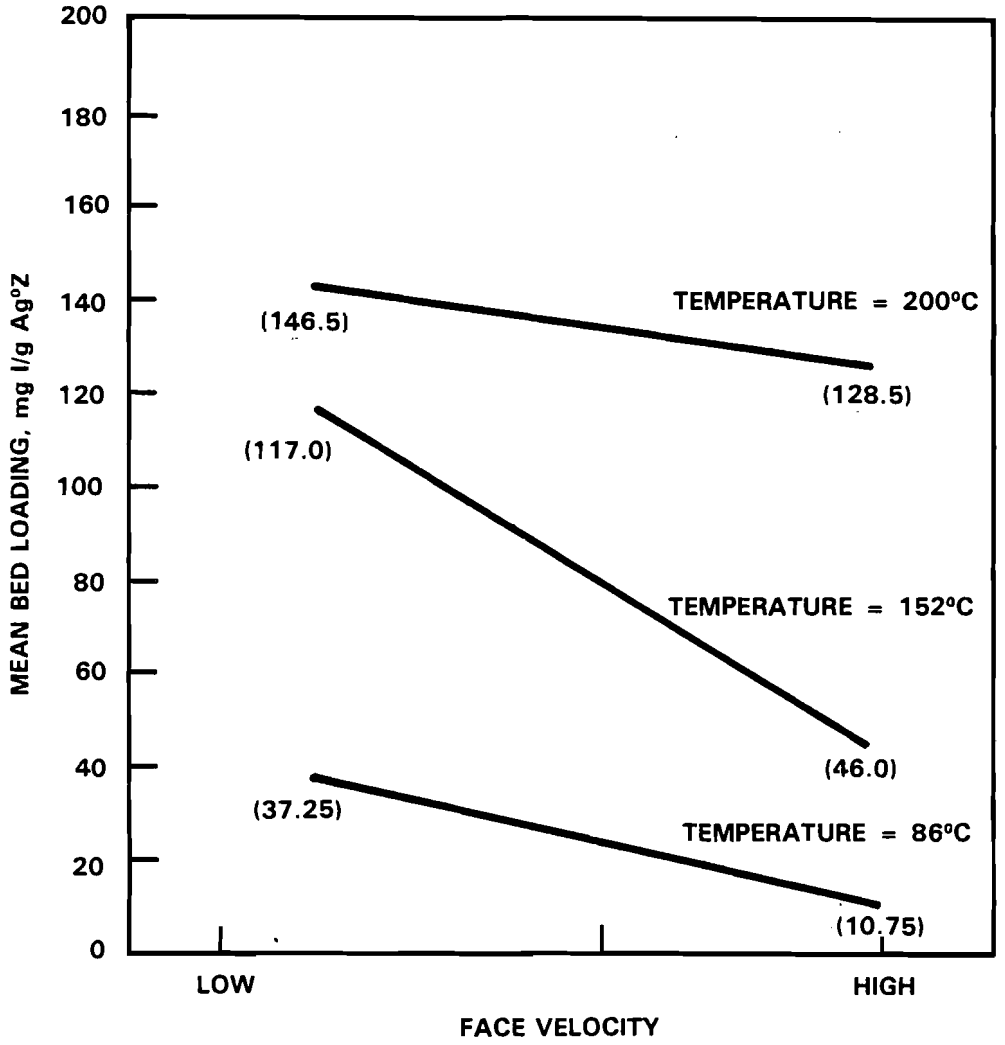

FIGURE 12. Phase 2 Analysis: The Effect of Face Velocity on CH_3I Capture by Ag°Z at 86, 152, and 200°C

CONCLUSIONS AND RECOMMENDATIONS

Our studies have shown the effectiveness of capturing CH_3I with AgZ that has been reduced (hydrogen pretreated). By extrapolation, Ag°Z should be an effective trap for other organic iodides found in the POG. The efficiency of CH_3I capture is dependent on various operational parameters and is affected by other gases in the POG of a nuclear reprocessing plant.

Maximum efficiency for the removal of CH_3I from gas streams by AgZ is obtained by small particle size, low face velocity, absence of NO, presence of water in the gas stream, and elevation of the temperature from 150 to around 200°C. Ag°Z is preferred over AgZ, and for the 10-16 mesh particles, a bed of at least 15 cm deep is suggested.

Complex interactions exist between the parameters investigated here. A better understanding of these might be obtained with a set of experiments using a relatively shallow bed and by observing the kinetics of capture rather than total bed loading.

Additional studies are recommended to improve knowledge on the basic chemistry of the sorption reaction of CH_3I and I_2 by silver zeolites.

REFERENCES

Addison, W. E. and R. M. Barrer. 1955. "Sorption and Reactivity of Nitrous Oxide and Nitric Oxide in Crystalline and Amorphous Siliceous Sorbents." Chem. Society Journal 757.

Barin, I. and O. Knacke. 1973. Thermochemical Properties of Inorganic Substances. Springer-Verlag, New York.

Barin, I., O. Knacke, and O. Kubaschewski. 1977. Thermochemical Properties of Inorganic Substances: Supplement. Springer-Verlag, New York.

Breck, D. W. 1974. Zeolite Molecular Sieves, Structure, Chemistry, and Use. John Wiley & Sons, New York.

Burger, L. L. and R. D. Scheele. 1981. "Iodine Fixation Studies at the Pacific Northwest Laboratory." In Management Modes for Iodine-129, W. Hebel and G. Cottone, eds. Harwood Academic Publishers, New York.

Burger, L. L. and R. D. Scheele. 1982. Recycle of Iodine-Loaded Silver Mordenite by Hydrogen Reduction. PNL-4490, Pacific Northwest Laboratory, Richland, Washington.

Chao, Chien-Chung, and J. H. Lunsford. 1971a. "Infrared Studies of the Disproportionation Reaction of Nitric Oxide on Y-Type Zeolites." JACS 93(1):71.

Chao, Chien-Chung, and J. H. Lunsford. 1971b. "Adsorption of Nitric Oxide on Y-Type Zeolites: A Low-Temperature Infrared Study." JACS 93(25):6794.

Coleman, J. E. and R. D. Scheele. 1981. "Scanning Electron Microscopy Studies." In "Iodine Fixation," Nuclear Waste Management Quarterly Progress Report, April through June 1981. PNL-3000-10, T. D. Chikalla and J. A. Powell, eds. Pacific Northwest Laboratory, Richland, Washington.

Daniel, J. L., J. E. Coleman, and R. D. Scheele. 1980. "Scanning Electron Microscopy Studies." In "Iodine Fixation," Nuclear Waste Management Quarterly Report, July through September 1980. PNL-3000-7, T. D. Chikalla and J. A. Powell, eds., Pacific Northwest Laboratory, Richland, Washington.

Donner, C. and T. Tamberg. 1971. "Zur Abscheidung von Methyl und Athyljodid an Silverzeolithen." P. 28, Atomwirtschaft, Jan 1971.

Donner, C. and T. Tamberg. 1972. "Zur Abscheidung Von Methyljodid an Silverzeolithen." Z. Naturforsch 27:1323-1328.

Glasstone, S. and G. Bell. 1946. Textbook of Physical Chemistry. 2nd ed. D. Van Nostrand Company, Inc., New York.

Hirschfelder, J. O., C. F. Curtiss, and R. B. Bird. 1954. Molecular Theory of Gases and Liquids. John Wiley & Sons, New York.

Jubin, R. T. 1982. "Organic Iodine Removal from Simulated Dissolver Offgas Systems Using Partially Exchanged Silver Mordenite." In Proceedings of the 17th Air Cleaning Conference, CONF-820833-12, National Technical Information Service, Springfield, Virginia.

Jubin, R. T. 1980. "Organic Iodine Removal from Simulated Dissolver Off-Gas Streams Using Silver-Exchanged Mordenite." In Proceedings of the 16th Air Cleaning Conference, CONF-801038, National Technical Information Service, Springfield, Virginia.

Kasai, P. H. and R. J. Bishop, Jr. 1972. "Electron Spin Resonance Study of Nitric Oxide Adsorption on Linde Type X Zeolites." JACS 94(16):5560.

Kennard, E. H. 1938. Kinetic Theory of Gases. McGraw-Hill, New York.

Latimer, W. M. 1956. Oxidation Potentials. 2nd ed. Prentice-Hall, Inc., Englewood Cliffs, New Jersey.

Meier, W. T. and D. H. Olson. 1971. "Zeolite Frameworks." In Molecular Sieve Zeolites, ed. R. F. Gould. Advances in Chemistry Series 101, American Chemical Society, Washington, D.C.

Minachev, K. H. and Y. I. Isakov. 1976. "Catalytic Properties of Metal-Containing Zeolites." In Zeolite Chemistry and Catalysis, ed. J. A. Rabo, pp. 552-611. ACS Monograph No. 171. American Chemical Society, Washington, D.C.

Murphy, L. P., B. A. Staples, and T. R. Thomas. 1977. The Development of Ag°Z for Bulk ^{129}I Removal from Nuclear Fuel Reprocessing Plants and PbX for ^{129}I Storage. ICP-1135, Idaho National Engineering Laboratory, Idaho Falls, Idaho.

Pietrzak, T. M. and D. E. Wood. 1970. "EPR Study of the Hindered Motion of NO_2 and ClO_2 Adsorbed in Synthetic Zeolites." J. Chem. Phys. 53(6):2454.

Scheele, R. D., 1981. "Silver Sorbent Characterization." In "Iodine-129 Fixation," Nuclear Waste Management Quarterly Progress Report, July-September 1981. PNL-3000-11, T. D. Chikalla and J. A. Powell, eds., Pacific Northwest Laboratory, Richland, Washington.

Scheele, R. D. and L. L. Burger. 1981. "Characterization Studies of Iodine-Loaded Silver Zeolites," PNL-SA-9510. Paper presented at the 182nd National Meeting of the American Chemical Society, August 23-28, 1981, New York.

Scheele, R. D., C. L. Matsuzaki, and L. L. Burger. 1981. "Iodine Recovery Studies." In "Iodine-129 Fixation," Nuclear Waste Management Quarterly Progress Report, April through June 1981. PNL-3000-10, T. D. Chikalla and J. A. Powell, eds. Pacific Northwest Laboratory, Richland, Washington.

Snedecor, G. W., and W. G. Cochran. 1980. Statistical Methods. 7th ed. Iowa State University Press, Ames, Iowa.

Strachan, D. M. 1978. Analysis of the Dissolver Silver Reactors from Hanford's Purex Plant. RHO-ST-2, Rockwell Hanford Operations, Richland, Washington.

Thomas, T. R., L. P. Murphy, B. A. Staples, and J. T. Nichols. 1977. Airborne Elemental Iodine Loading Capacities of Metal Zeolites and a Method for Recycling Silver Zeolite. ICP-1119, Idaho National Engineering Laboratory, Idaho Falls, Idaho.

Wiemers, K. D. 1978. "Iodine Recovery Studies," Nuclear Waste Management Quarterly Progress Report, October through December 1978. PNL-2378-4, A. M. Platt and J. A. Powell, eds., Pacific Northwest Laboratory, Richland, Washington.

Wiemers, K. D. and R. D. Scheele. 1979. "Iodine Recovery." In "Carbon-14 and Iodine-129 Fixation," Nuclear Waste Management Quarterly Progress Report, April through June 1979. PNL-3000-2, A. M. Platt and J. A. Powell, eds., Pacific Northwest Laboratory, Richland, Washington.

APPENDIX A

CH_3I LOADING CURVES

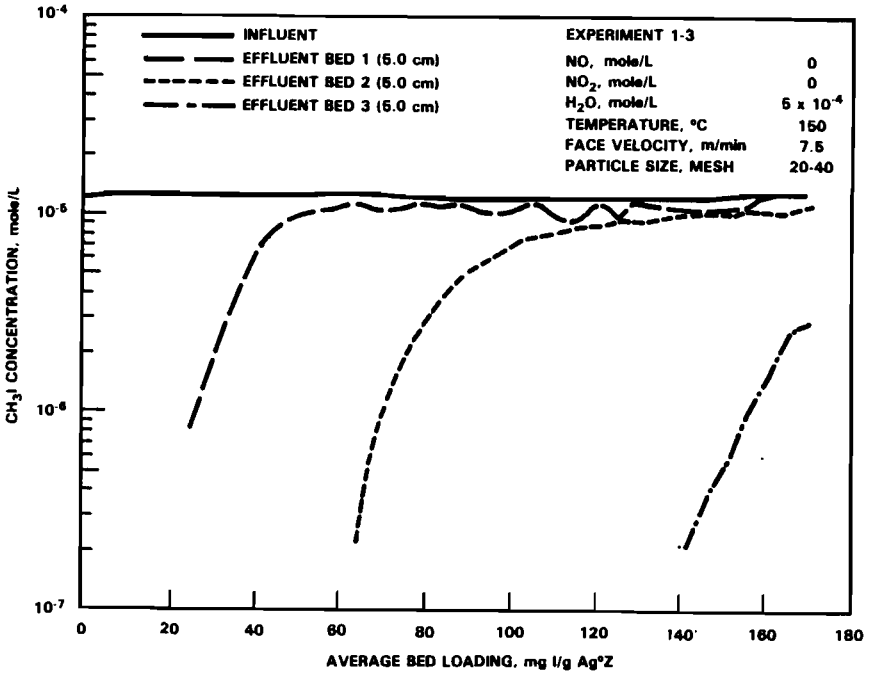

FIGURE A.1. CH_3I Capture by Ag°Z, Experiment 1-3

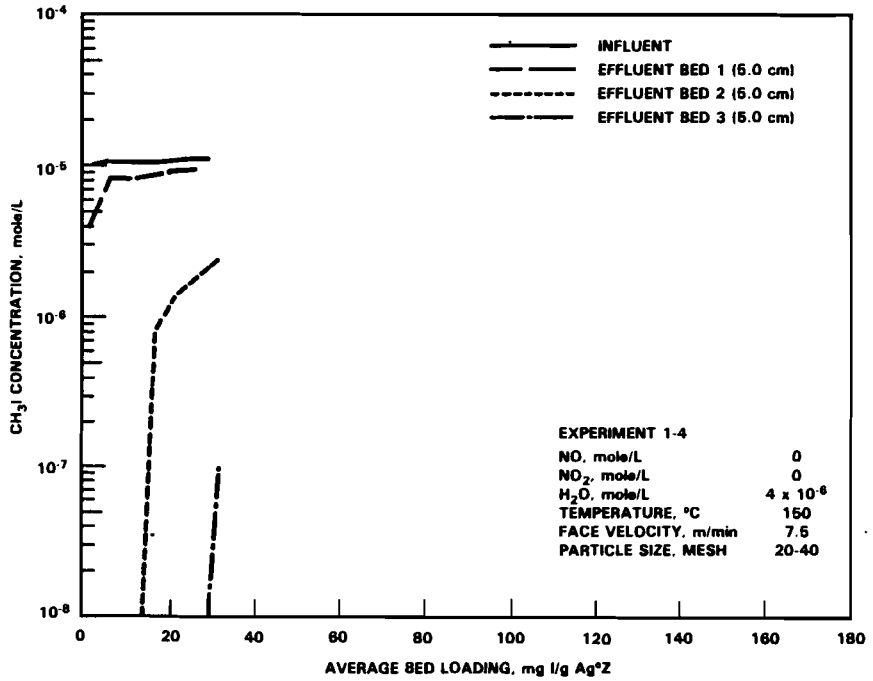

FIGURE A.2. CH_3I Capture by Ag°Z, Experiment 1-4

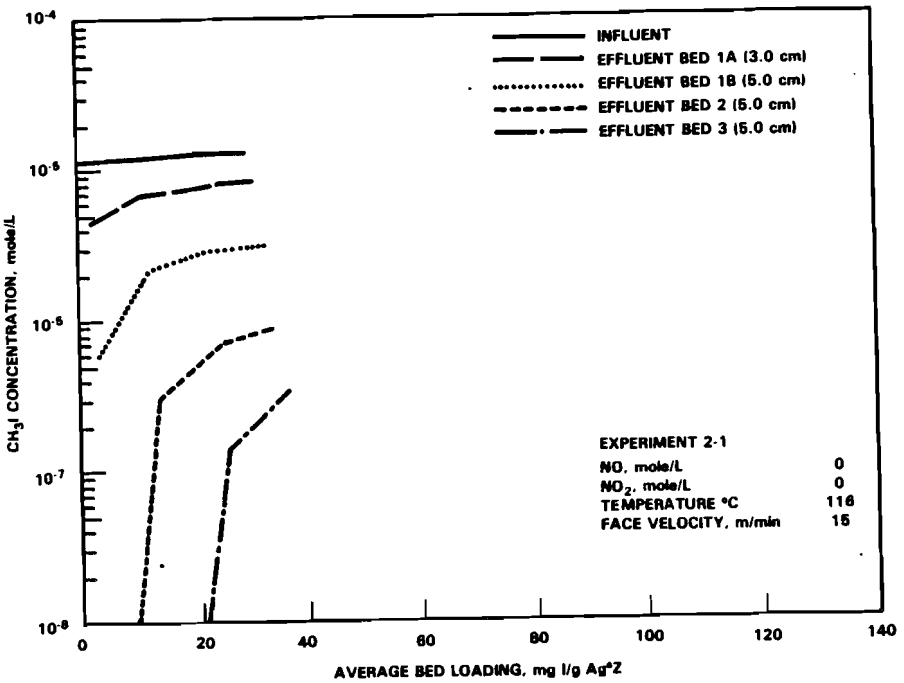

FIGURE A.3. CH_3I Capture by Ag°Z, Experiment 2-1

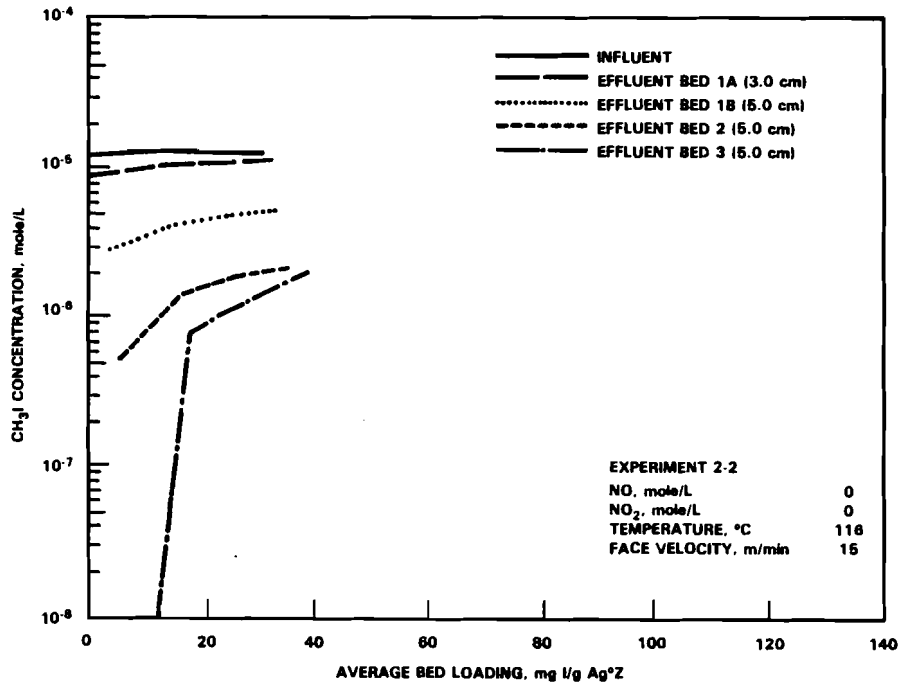

FIGURE A.4. CH_3I Capture by Ag°Z, Experiment 2-2

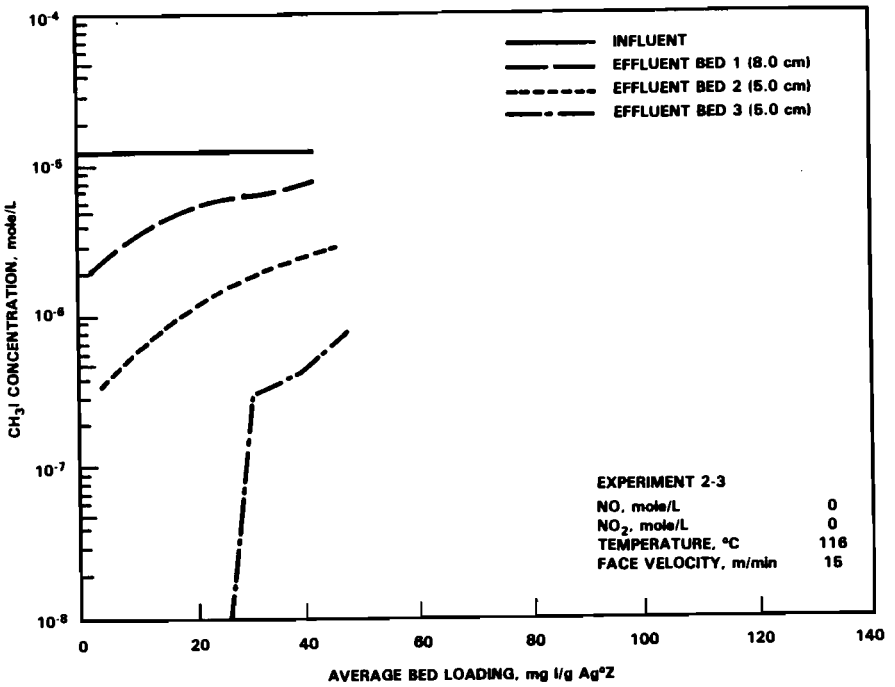

FIGURE A.5. CH_3I Capture by Ag°Z, Experiment 2-3

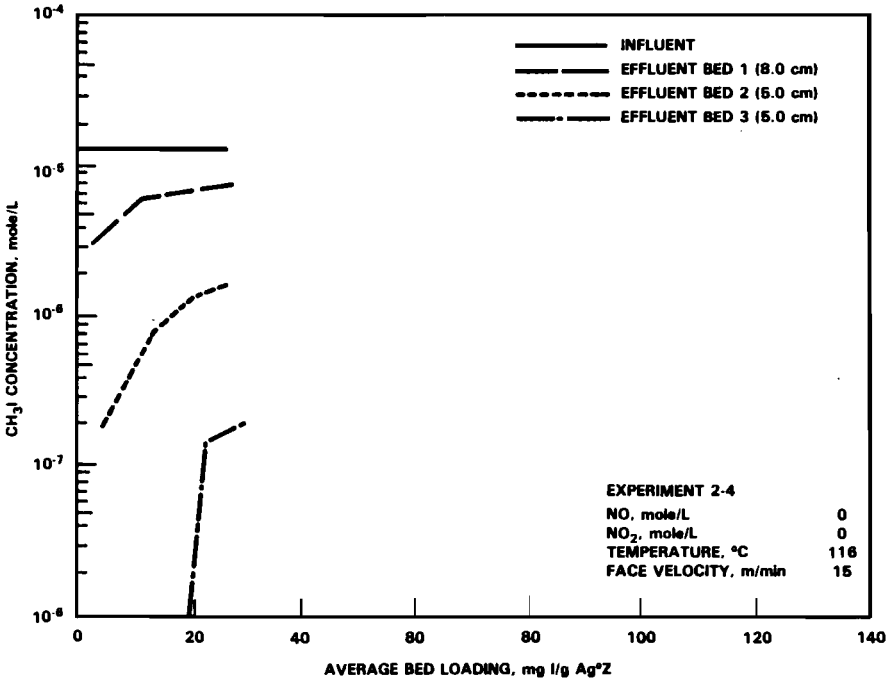

FIGURE A.6. CH_3I Capture by Ag°Z, Experiment 2-4

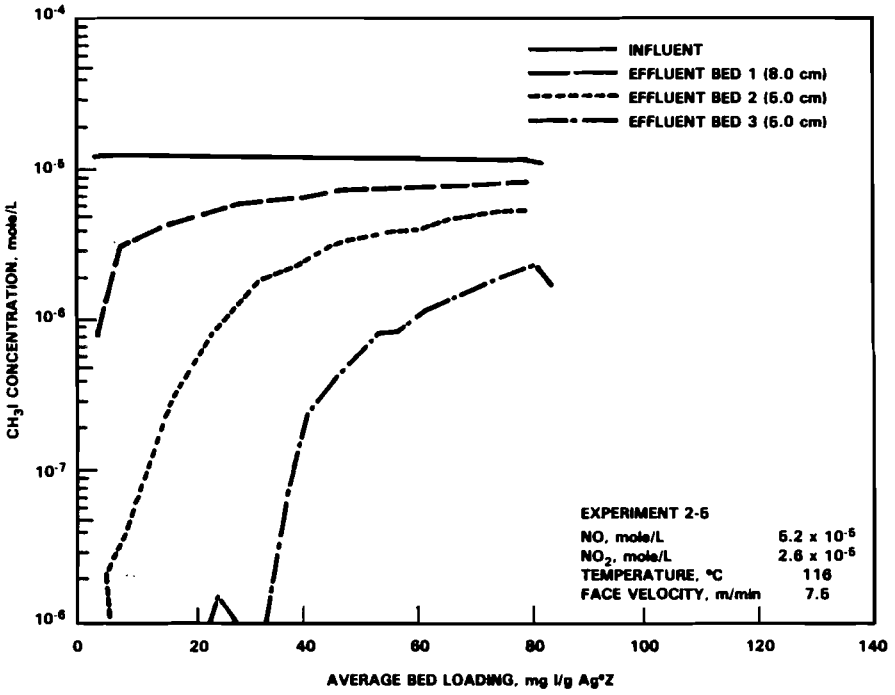

FIGURE A.7. CH_3I Capture by Ag°Z, Experiment 2-5

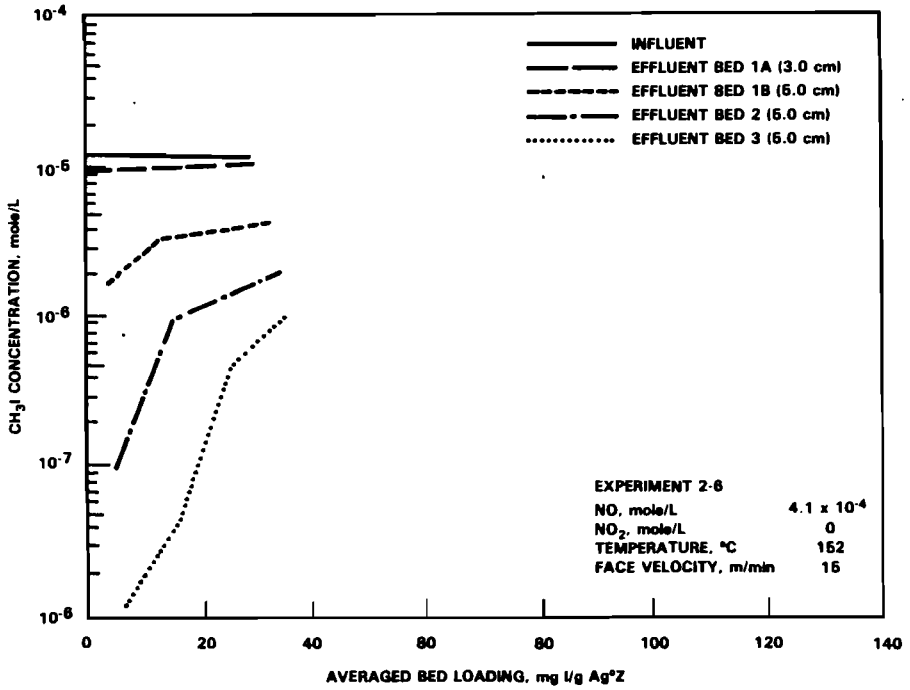

FIGURE A.8. CH_3I Capture by Ag°Z, Experiment 2-6

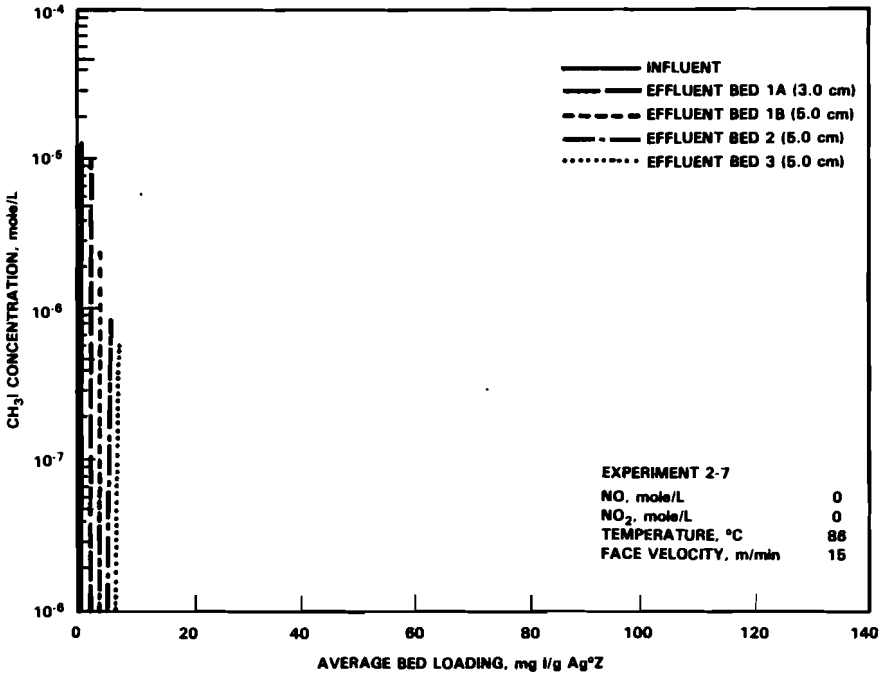

FIGURE A.9. CH_3I Capture by Ag°Z, Experiment 2-7

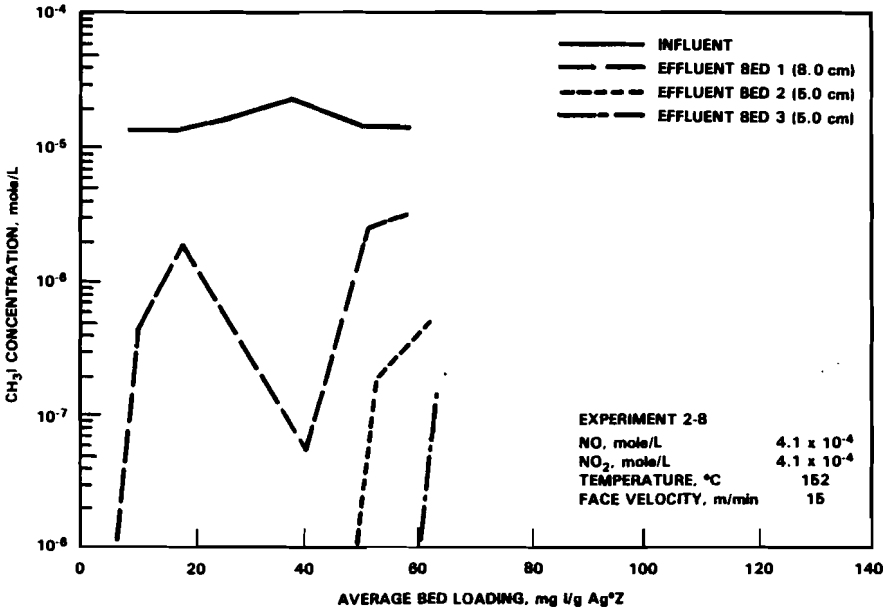

FIGURE A.10. CH_3I Capture by Ag°Z, Experiment 2-8

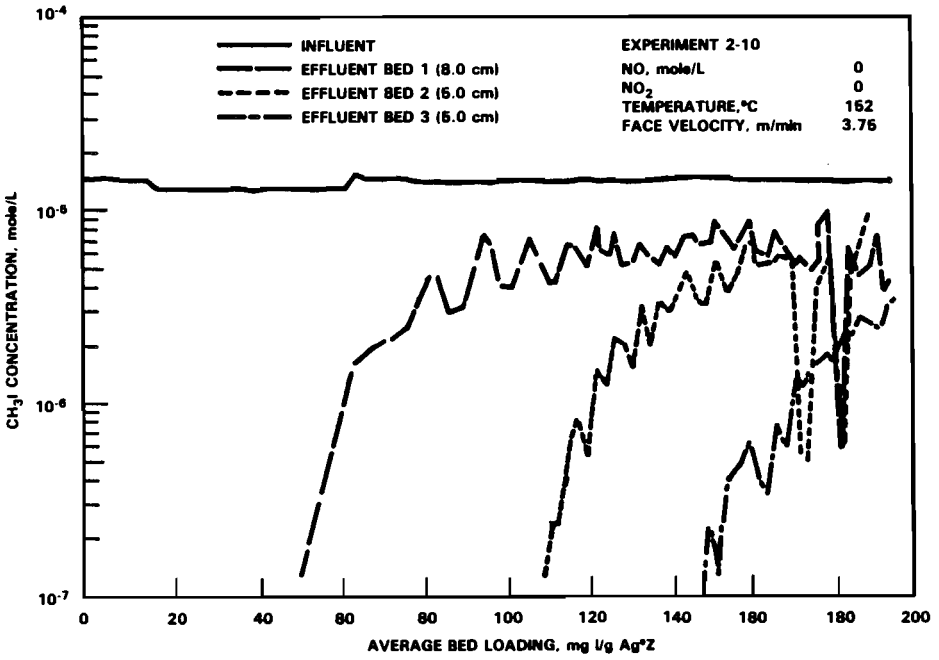

FIGURE A.11. CH_3I Capture by Ag°Z, Experiment 2-10

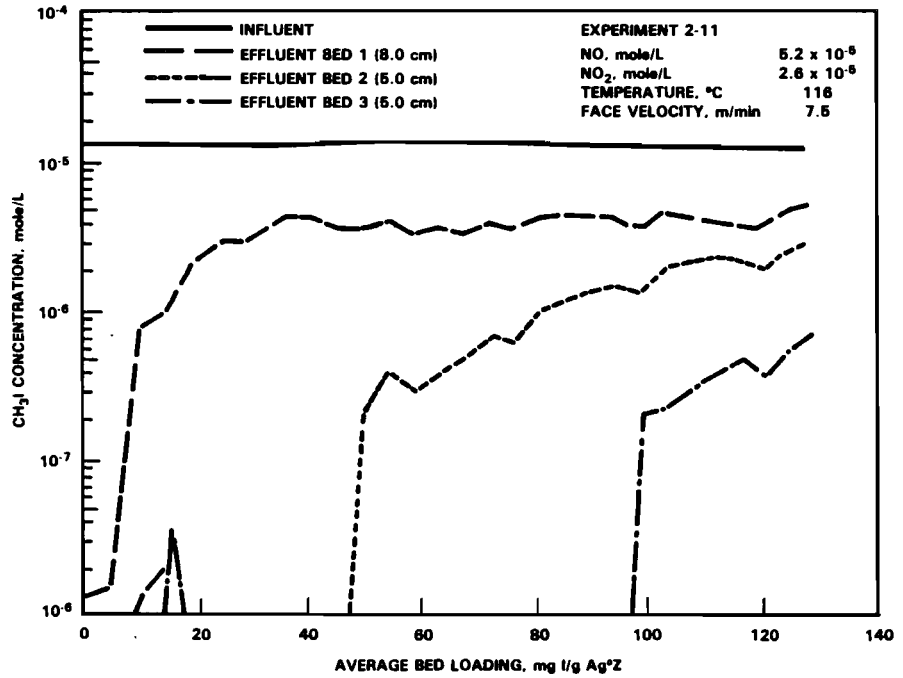

FIGURE A.12. CH_3I Capture by Ag°Z, Experiment 2-11

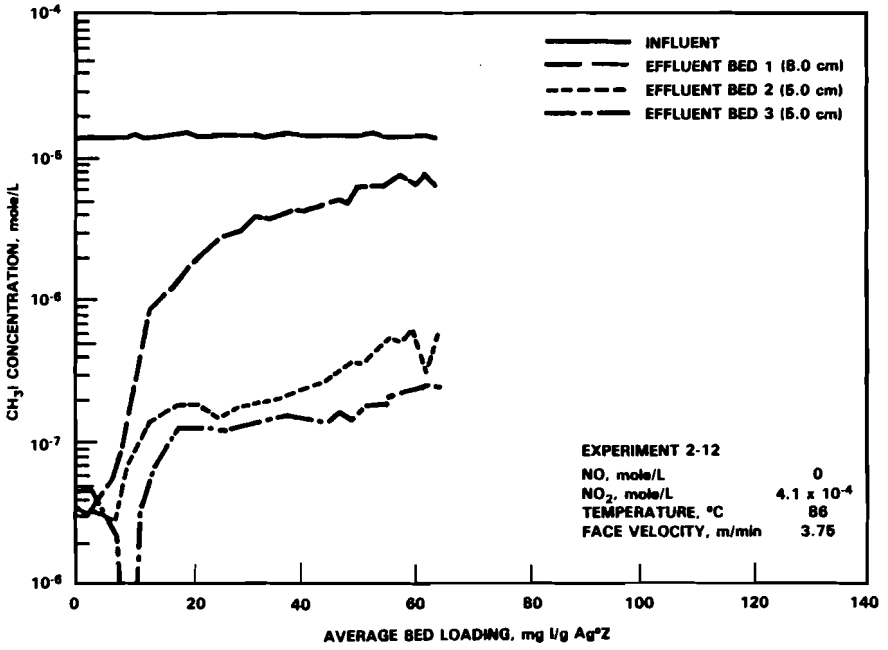

FIGURE A.13. CH_3I Capture by Ag°Z, Experiment 2-12

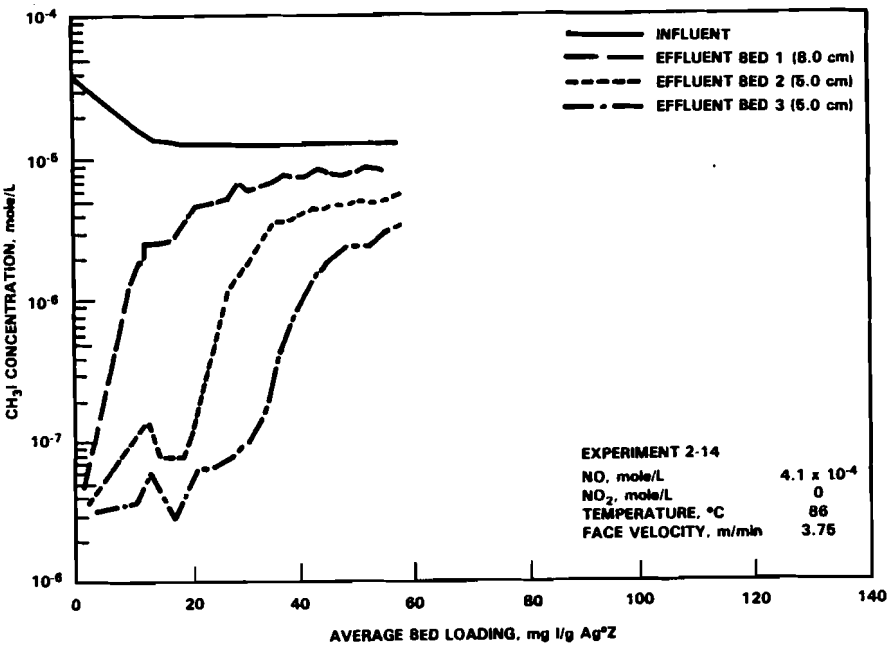

FIGURE A.14. CH_3I Capture by Ag°Z, Experiment 2-14

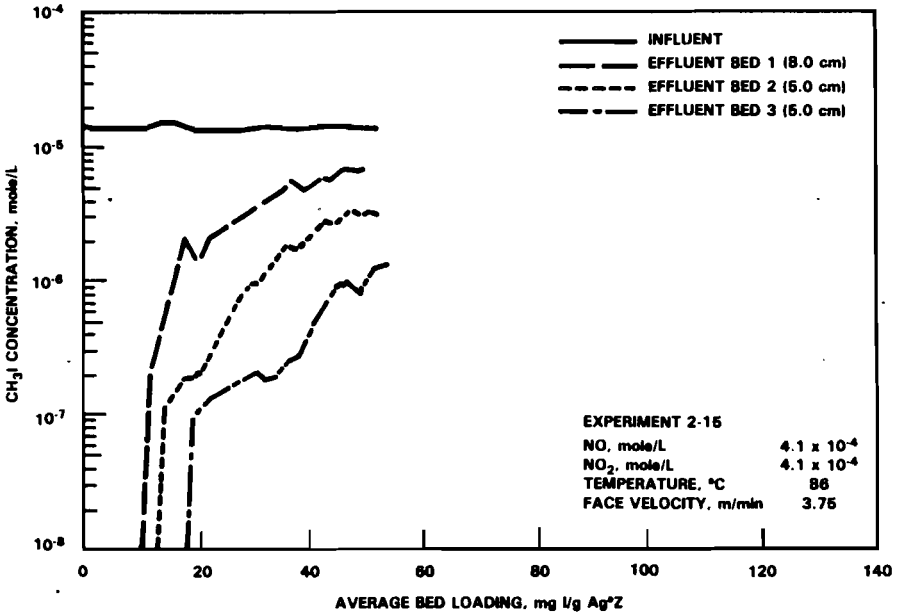

FIGURE A.15. CH_3I Capture by Ag°Z, Experiment 2-15

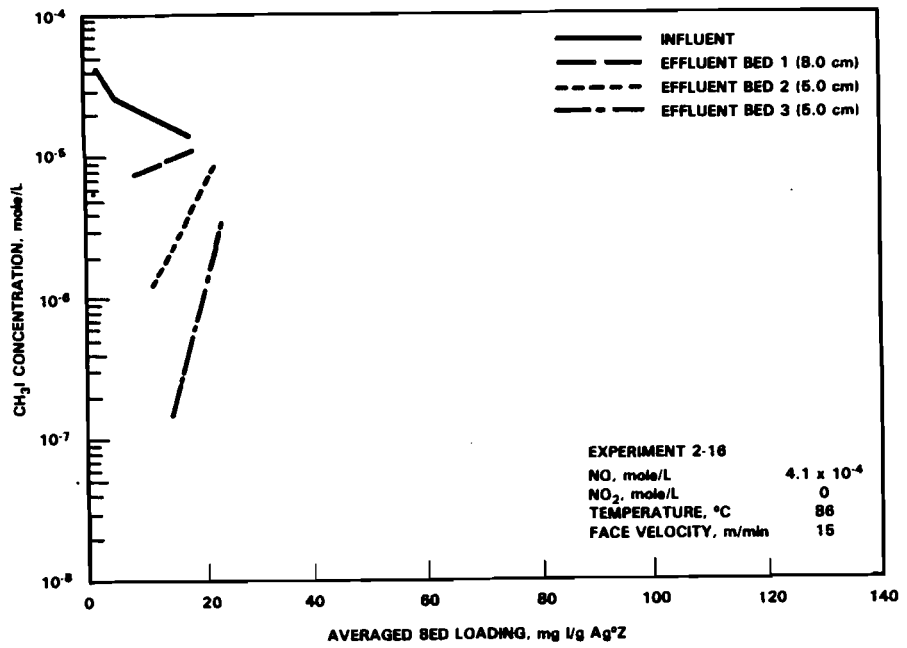

FIGURE A.16. CH_3I Capture by Ag°Z, Experiment 2-16

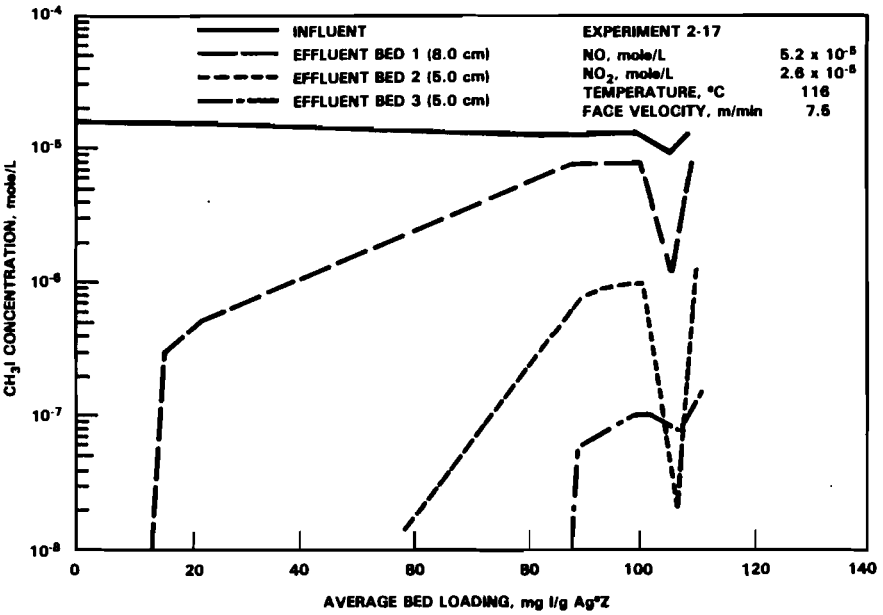

FIGURE A.17. CH_3I Capture by Ag°Z, Experiment 2-17

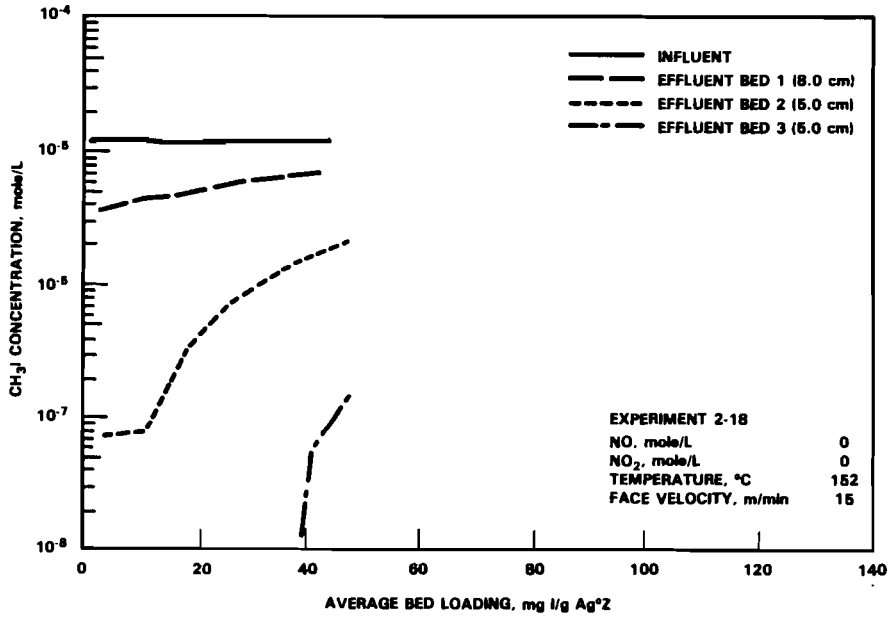

FIGURE A.18. CH_3I Capture by Ag°Z, Experiment 2-18

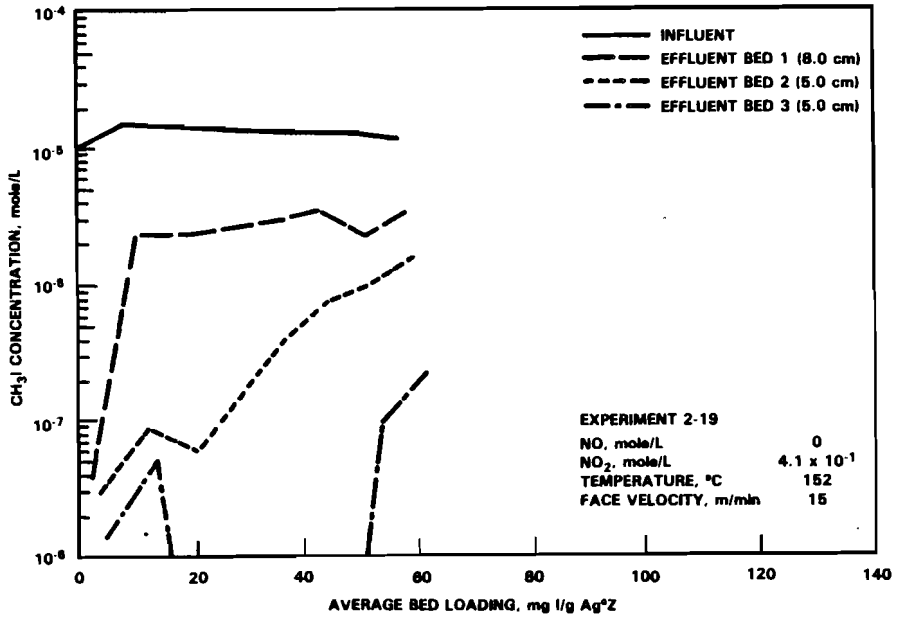

FIGURE A.19. CH_3I Capture by Ag°Z, Experiment 2-19

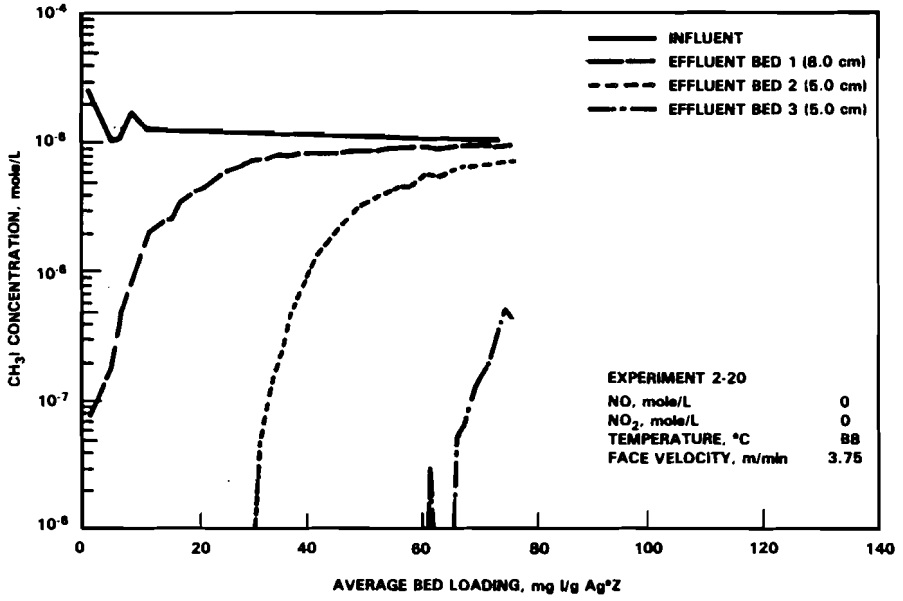

FIGURE A.20. CH_3I Capture by Ag°Z, Experiment 2-20

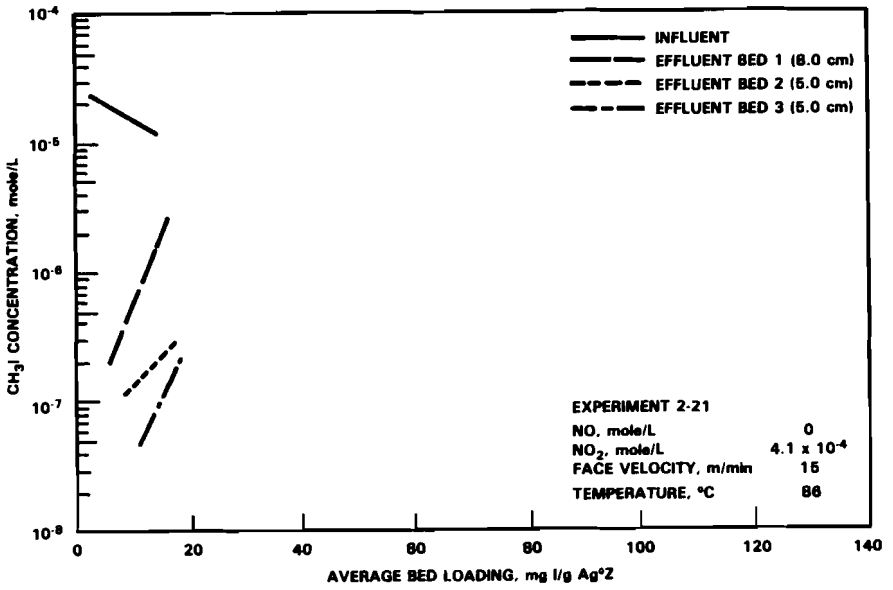

FIGURE A.21. CH_3I Capture by Ag°Z, Experiment 2-21

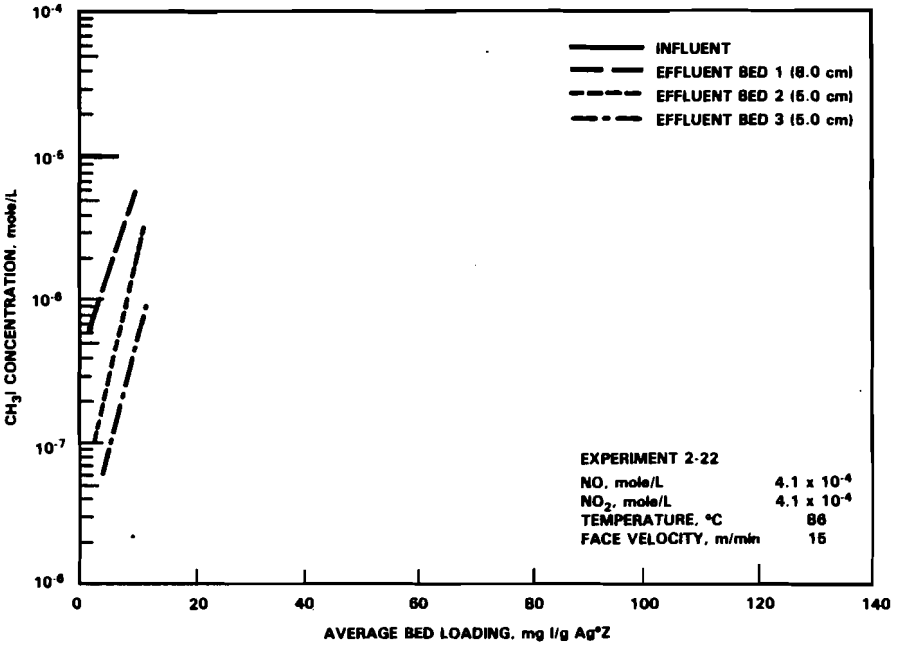

FIGURE A.22. CH_3I Capture by Ag°Z, Experiment 2-22

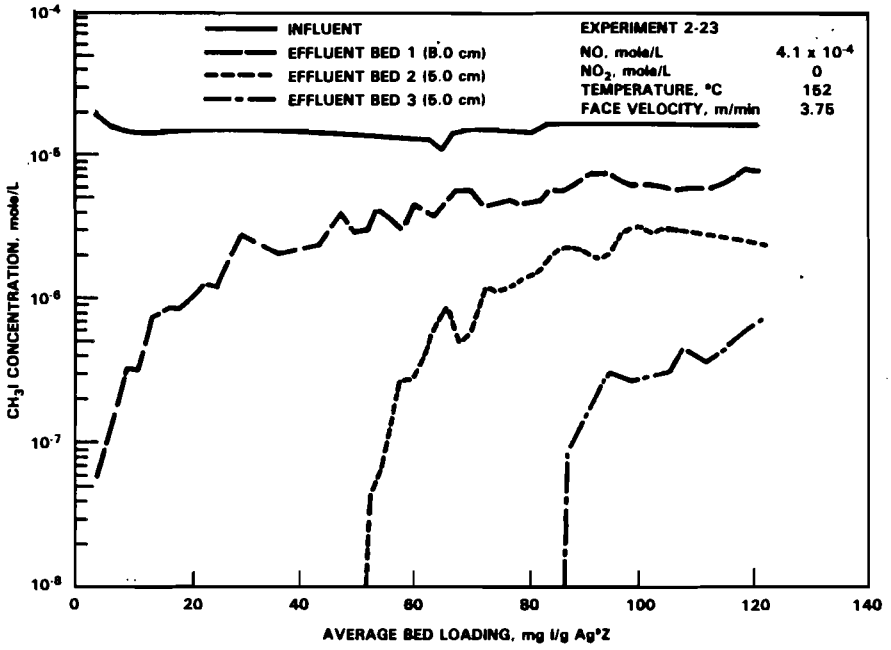

FIGURE A.23. CH_3I Capture by Ag°Z, Experiment 2-23

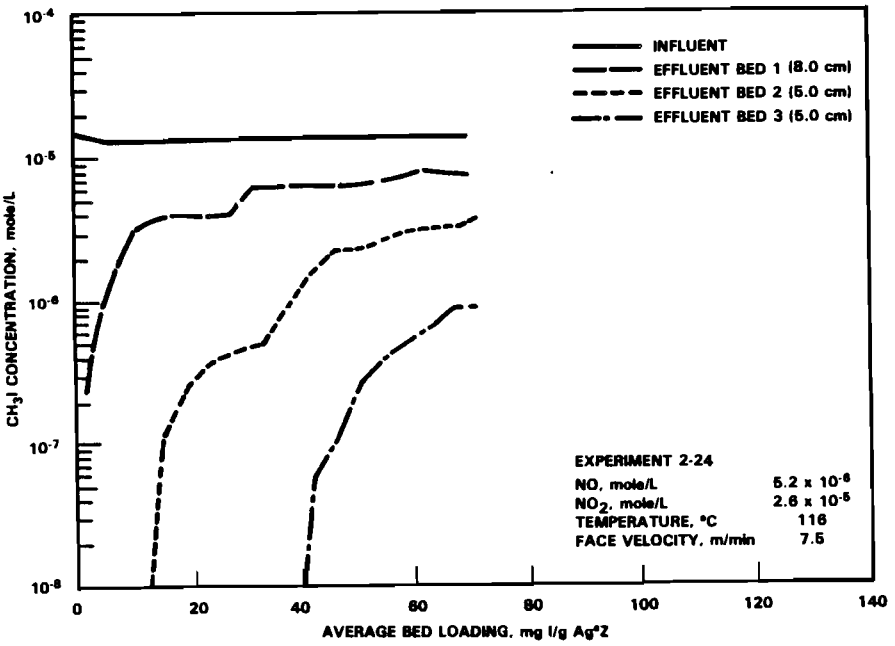

FIGURE A.24. CH_3I Capture by Ag°Z, Experiment 2-24

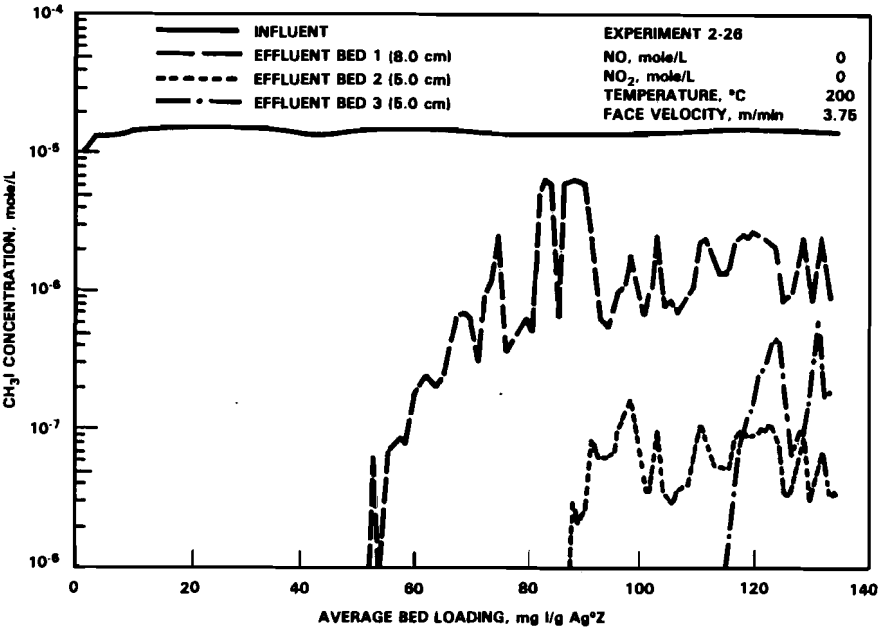

FIGURE A.25. CH_3I Capture by Ag°Z, Experiment 2-26

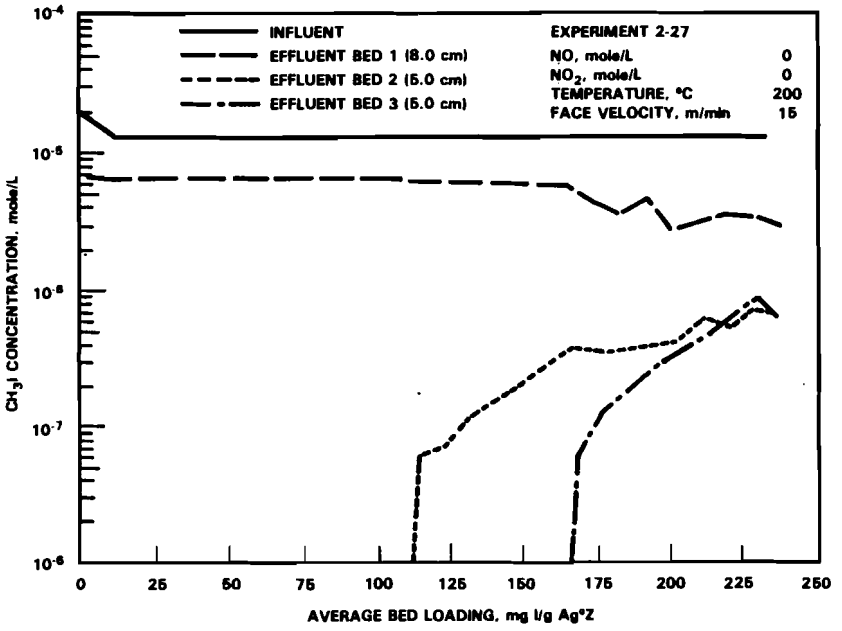

FIGURE A.26. CH_3I Capture by Ag°Z, Experiment 2-27

DISTRIBUTION

No. of Copies

OFFSITE

27 DOE Technical Information Center

R. E. Cunningham
Office of Nuclear Safety
Materials and Safeguards
Room 562
Nuclear Regulatory Commission
7915 Eastern Avenue
Silver Springs, MD 20910

3 Division of Waste Management
Nuclear Regulatory Commission
Washington, DC 20555
ATTN: J. B. Martin
D. B. Rohrer
R. D. Smith

Materials Section Leader
High Level Waste Licensing
Branch
Nuclear Regulatory Commission
Washington, DC 20555

W. E. Mott
DOE Division of Environmental
Control Technology
EV-13, GTN
Washington, DC 20545

3 DOE Office of Terminal Waste
Disposal and Remedial Actions
NE30, GTN
Washington, DC 20545
Attn: F. E. Coffman
J. R. Coleman
J. A. Turi

No. of Copies

4 DOE Office of Spent Fuel
Management and Reprocessing
Systems
Washington, DC 20545
Attn: N. W. Ballard
C. B. Bastin
K. O. Laughon
W. H. McVey

3 DOE Office of Defense Waste and
Byproducts Management
DP-12, GTN
Washington, DC 20545
ATTN: T. C. Chee
G. Oertel
R. D. Walton

2 Geologic Repository Division
Nuclear Waste Policy Act
Project Office: DOE
S-10 Forrestal Bldg.
Washington, DC 20585
ATTN: J. W. Bennett
M. J. Lawrence

C. R. Cooley
Geologic Repository Division
Nuclear Waste Policy Act
S-10/NE-22 GTN
Washington, DC 20585

Environmental Protection Agency
Technological Assessment
Division (AW-559)
Office of Radiation Programs
Washington, DC 20460

No. of Copies

S. A. Mann
DOE Chicago Operations and Region Office
Argonne, IL 60439

J. O. Neff
DOE Columbus Program Office
505 King Avenue
Columbus, OH 43201

3 DOE Idaho Operations Office
550 Second Street
Idaho Falls, ID 83401
Attn: J. P. Hamric
J. B. Whitsett
M. A. Widmayer

Office of the Assistant Manager for Energy Research and Development
DOE Oak Ridge Operations Office
P. O. Box E
Oak Ridge, TN 37830

3 DOE Savannah River Laboratory
P.O. Box A
Aiken, SC 29801
ATTN: E. S. Goldberg
T. B. Hindman
R. B. Whitfield

R. Y. Lowrey
DOE Albuquerque Operations Office
P. O. Box 5400
Albuquerque, NM 87185

S. G. Harbinson
DOE San Francisco Operations Office
1333 Broadway
Oakland, CA 94612

No. of Copies

W. F. Holcomb
National Institute of Health
Radiation Safety Branch
Building 21
Bethesda, MD 20205

2 Allied-General Nuclear Services
P. O. Box 847
Barnwell, SC 29812
ATTN: J. A. Buckham
A. Williams

2 Argonne National Laboratory
9700 South Cass Avenue
Argonne, IL 60439
ATTN: J. H. Kittel
M. J. Steindler/
L. E. Trevorrow

9 Battelle Memorial Institute
505 King Avenue
Columbus, OH 43201
ATTN: S. H. Basham
A. Carbiener
N. E. Carter
J. O. Duguid
S. Goldsmith
P. L. Hofmann
M. Kehnemuyi
J. F. Kircher
B. Rawles

2 EG&G Idaho, Inc.
P. O. Box 1625
Idaho Falls, ID 83415
ATTN: G. B. Levin
R. L. Tallman

R. Williams
Electric Power Research Institute
3412 Hillview Avenue
P. O. Box 10412
Palo Alto, CA 94304

No. of
Copies

Exxon Nuclear Idaho
P. O. Box 2800
Idaho Falls, ID 83401
ATTN: R. A. Brown
J. D. Christian
T. R. Thomas

6 Oak Ridge National Laboratory
P.O. Box X
Oak Ridge, TN 37830
ATTN: J. O. Blomeke
W. D. Burch
A. G. Croff
R. J. Jubin
R. G. Wymer
T. H. Row

7 E. I. duPont deNemours & Co. Inc.
Savannah River Laboratory
Aiken, SC 29801
ATTN: H. H. Baker
M. D. Boersma
J. L. Crandall
S. D. Harris
D. L. McIntosh
S. Mirshak
S. W. O'Rear

E. Vejvoda
Rockwell International
Rocky Flats Plant
P. O. Box 464
Golden, CO 80401

2 GA Technologies
P. O. Box 81608
San Diego, CA 92138
ATTN: G. E. Benedict
W. S. Scheib, Jr.

J. L. Larocca, Chairman
Energy Research and Development Authority
Empire State Plaza
Albany, NY 12223

No. of
Copies

2 Lawrence Livermore Laboratory
P. O. Box 808
Livermore, CA 94550
ATTN: J. H. Campbell
W. G. Sutliff

3 Sandia Laboratories
Albuquerque, NM 87185
Attn: O. E. Jones
R. G. Kepler
W. Weart

R. Roy
202 Materials Research Laboratory
University Park, PA 16802

J. R. Potter
Chem-Nuclear Systems, Inc.
P. O. Box 1866
Bellevue, WA 98009

R. G. Post
College of Engineering
University of Arizona
Tucson, AZ 85721

W. A. Freeby
Bechtel Group, Inc.
Fifty Beale Street
P. O. Box 3965
San Francisco, CA 94119

L. L. Hench
Dept. of Materials Science and Engineering
University of Florida
Gainesville, FL 32611

H. Palmour III
2140 Burlington Engineering Laboratories
North Carolina State University
Raleigh, NC 27607

No. of Copies

W. Tope
Westinghouse Electric Corporation
Penn Center, Building 2
Box 355
Pittsburgh, PA 15230

ONSITE

4 DOE Richland Operations Office

P. F. X. Dunigan, Jr.
H. E. Ranson
J. J. Schreiber (2)

13 Rockwell Hanford Operations

J. L. Deichman
J. O. Honeyman
L. Jensen
J. E. Kinser
H. G. McGuire
R. M. Orme
J. Reser
J. H. Roecker
W. W. Schulz
R. E. Van der Cook
D. G. Wilkins
G. D. Wright
File Copy

2 UNC United Nuclear Industries

F. H. Bouse, Document Control
T. E. Dabrowski

Westinghouse Hanford Company

3 A. G. Blasewitz
R. E. Lerch
J. J. McCown

No. of Copies

67 Pacific Northwest Laboratory

W. F. Bonner
F. P. Brauer
L. A. Bray
L. L. Burger (15)
T. D. Chikalla
C. R. Hann
O. F. Hill
J. H. Jarrett
A. B. Johnson, Jr.
S. E. King
M. R. Kreiter
L. T. Lakey
R. C. Liikala
R. P. Marshall
E. D. McClanahan
J. L. McElroy
J. E. Mendel
I. C. Nelson
J. M. Nielsen/R. W. Perkins
R. E. Nightingale
A. M. Platt
W. A. Ross
J. M. Rusin
R. D. Scheele (15)
J. K. Soldat
J. L. Swanson
G. L. Tingey
C. L. Unruh
H. H. Van Tuyl
E. C. Watson
E. J. Wheelwright
W. R. Wiley
Technical Information (5)
Publishing Coordination (2)